Research article

Applying of SP, DC-Resistivity, DC-TDIP and TDEM soundings in high saline coastal aquifer

A.I. Ammar [a,*], M. Gomaa [b], K.A. Kamal [a]

[a] Research Institute for Groundwater, National Water Research Center, Cairo, Egypt
[b] Geophysical Science Departments, National Research Centre, Cairo, Egypt

ARTICLE INFO

ABSTRACT

Four surface geophysical techniques were utilized to study the geological and hydrogeological settings of highly saline a coastal aquifer system to the north-east of River Nile Delta, Egypt. These techniques include SP, DC-Resistivity, TDIP and TDEM methods. The first target was to determine the geological stratification as a differentiation among clay, clayey, sand and sandy layers of high saline water. These techniques reflect that there is a complicated lateral and vertical difference in sediments along study area. The surface layers with depth down to ~120 m have low to medium content of clay that change with depth. Then, the second target was the differentiation laterally and vertically for salinity with depth down to ~250m as an interesting hydrogeological setting. These techniques reported that the sediments consist of thin and thick clay and silts, clayey sand, and sandy clay strata. Investigation depth was up to ~210m due to high salinity and clay content effect. At shallow depths, soil texture (down to ~100m and sometimes down to ~160m) consists of clay and silt with sand intercalation. The TEM data indicate a zone of less saline water and low clay content starting from ~40 to ~100m. There may be an evidence for a significant high to medium clay content after these depths down to ~250m. All four methods were calibrated with each other. Accordingly, good matching between the inversion model of TEMSs and composite logs of new drilled well was found, especially in lithological layers identifications. Also, this calibration confirmed that the area was complicated regarding the geological and hydrogeological conditions and the TDIP and TEM are the best methods in studying the environmental, geological and hydrogeological settings as primary important engineering implications for studying coastal highly saline aquifers.

1. Introduction

The geophysical methods used as integrated methods in this study were not to explore the groundwater aquifer, but for investigating the subsurface geological layers of the site in the form of geological units and soil texture, which are an important geological setting in the coastal plain (Erol, 1989), in addition to the hydrogeological conditions of these units as an engineering implication for engineering geology and hydrogeology in complex, high saline coastal areas. Therefore, for achieving these goals, the electrical properties of these units with emphasis on their resistivity and/or conductivity are the main physical properties measured by these methods.

In general, differentiation laterally and vertically between the complicated subsurface geological sediments such as clayey and non-clayey sediments in high saline water areas is not easy task and is an important and difficult target for Groundwater Engineering and Geology

for avoiding surface and subsurface collapses or subsidence during drilling, groundwater withdrawal and construction as well as for making a geological model to simulate the general and primary subsurface geological and geotechnical conditions. Therefore, the geophysical methods used in this study will assist in solving various subsurface geological and hydrogeological engineering problems such as the ambiguity between clay and saline water and how to solve the effect of salt water on these methods during measurement for avoiding this ambiguity. Accordingly, these methods together with the well logging data and lithology from wells assisted in depicting the geological setting of subsurface sediments in such complex subsurface conditions along the study area with emphasis on recording depths of high silt and clay content.

The integration surface geophysical methods are ideal for relatively homogenous water-bearing layers when the geological site is simple but less effective at the geological complex site (Parks et al., 2011) such as the area under study due to the presence of many complex subsurface

---

* Corresponding author.
E-mail address: abdallah_ammar@nwrc.gov.eg (A.I. Ammar).

conditions, such as lateral and vertical variation in the content of clay and silt with highly saline water which has a greater influence on the measurements of geophysical methods. Therefore, we used different methods to overcome this problem and get the best picture for the geological setting of the site examined.

Geophysical methods are widely used for non-intrusive monitoring of groundwater (Choudhury et al., 2001; Kafri and Goldman, 2005; Balia et al., 2009; Balia and Viezzoli, 2015). There are several authors who have used several geophysical methods such as TEM for delineating the coastal aquifers (Nowroozi et al., 1999; Yang et al., 1999; Shtivelman and Goldman, 2000; Manheim et al., 2004). Due to confusion of resistivity values between clay and saline water, some authors use seismic methods (Shtivelman and Goldman 2000), and others use calibration between core samples and logs (Manheim et al., 2004) for solving this problem. Nowroozi et al. (1999) argue that this problem cannot be solved at all. The implementation of IP (Induced Polarization) for environmental hydrogeology shows a sharp increase at the last 50 years. In general, there are few cases of application of hydro-geophysical models in coastal areas (Slater and Sandberg, 2000; Slater and Lesmes, 2002).

This study is an approach to characterize the hydro-geophysical properties of costal aquifers by integrating shallow Spontaneous Polarization (SP), DC-resistivity (VESs), DC Time-Domain Induced Polarization (DC-TDIPs) and deep Time-Domain (Transient) Electromagnetic (TDTEMs) geophysical techniques to solve the problem of clay/saline water correlation and to overcome effect of penetration depth of high salinity using resistivity methods.

SP, DC-Resistivity, and DC-TDIP soundings were used for separating and distinguishing thin clay and non-clay layers, particularly at shallow depths (~100 m depth). TEMs penetrate to deep depths (>~200m) and separate between thick clay or clayey layers. These methods are very useful in distinguishing between salt and fresh water and to determine the interface between salt-fresh water. Therefore, the four methods complement each other and combined together to overcome the effect of high salinity. Also, the sounding technique is very complex and not easy for solving this problem as a complex environmental problem, because it needs high accuracy in measurement and interpretation. This target was

very difficult because the used methods were applied close to the shore and over the sediments saturated with brine water.

2. Geology

The surface geological sediments around the study area consist of Nile River silt, Sabkha, sand dunes, stabilized dunes and undifferentiated quaternary deposits as shown by the map (Figure 1, left). The age of these sediments is Quaternary. The predominant distribution of these sediments is Nile silt, which is concentrated in the west of the research area and in some parts to the south of it, and consists of silty sand and sandy clay. The age of this silt is Holocene epoch. The main composition of the surface sediments of the research area is sand of various grain sizes (Holocene age). Undifferentiated Quaternary deposits occur in small portions of the NWN and are composed of sand, clay and silt. They are mainly Wadi deposits, alluvial fan deposits, desert detritus and desert crust and they belong to the Pleistocene age. Sabkha deposits are also found and distributed south of the research area and in some parts to the west. The last deposits are collected from fine silty deposits mixed with salt, due to evaporation of brine water.

Subsurface geological sediments, according to geological column (Figure 1, right, Said, 1981), consist of several stratigraphic units and are as follows:

1 **Bilqas Formation (Quaternary, Holocene age)**

This formation belongs to Neonile deposits which consist of alternating fine to medium–grained sand, clay interbeds with silt with thickness of ~50 m.

2 **Mit Ghamer Formation (Quaternary, Middle Pleistocene age)**

These Prenile deposits consist of sand pebble beds with few minor clay interbeds at lower part with thickness of ~700 m. This formation is present with more details at well (1) located to the south of the research area (Figure 2, left).
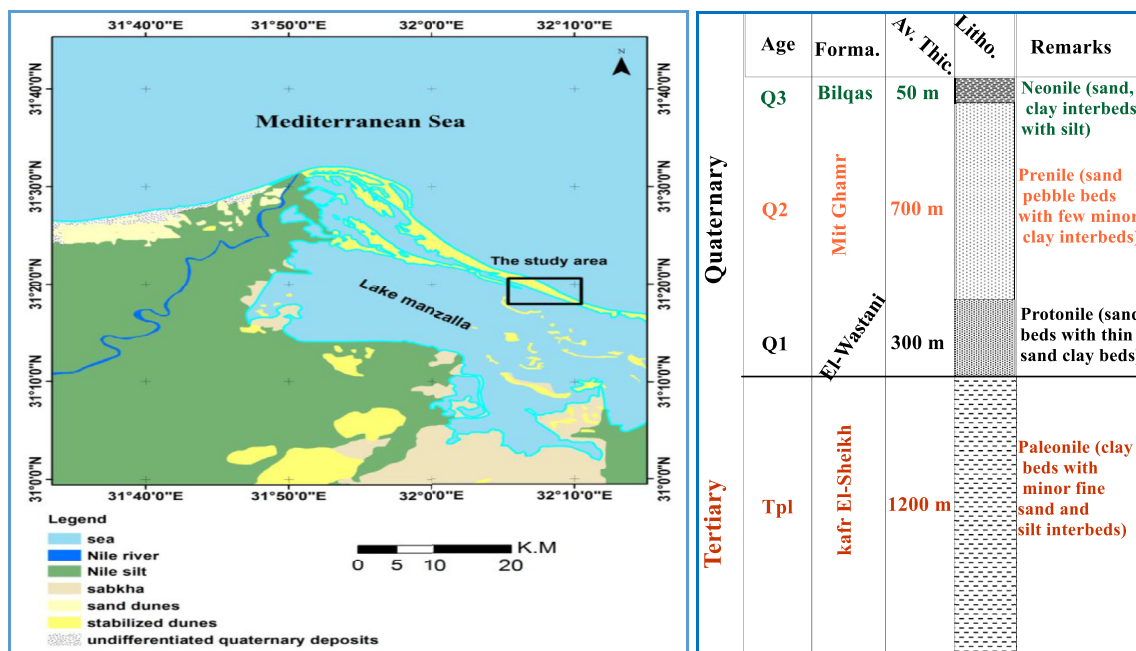
Figure 1. Geological map of the northern east part of River Nile Delta including the study area (data and factual information obtained from Klitsch et al., 1987), Left panel, and Composite columnar section of the main subsurface geological formations of the research area (data and factual information obtained from Said, 1981), Right panel.
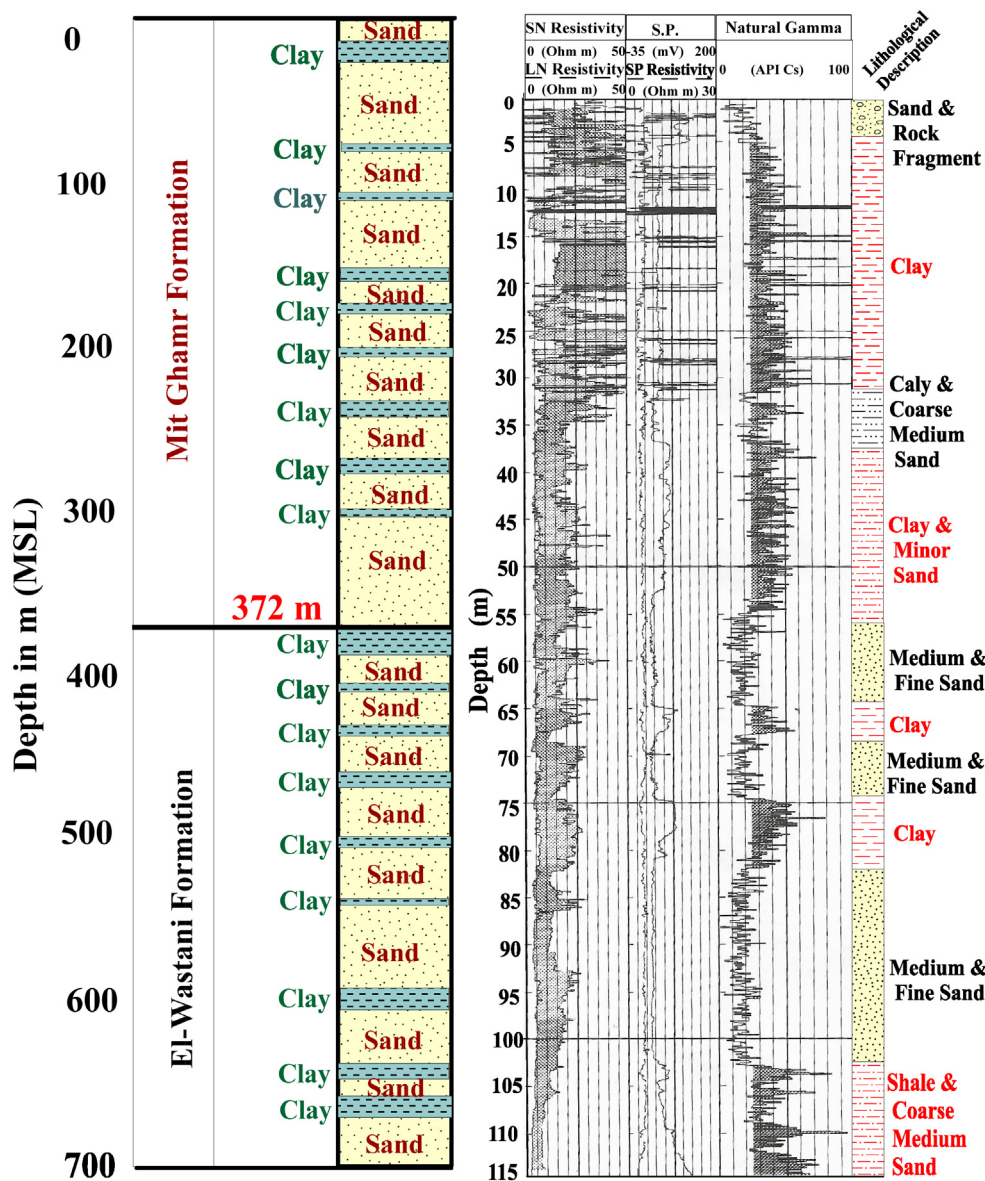
Figure 2. Thickness and sediments of Mit-Ghamr and Wastani Formations at well 1 (700m) South of study area (left panel), the Composite Short and Long Resistivity, Single Point Resistivity, Self-Potential, Gamma Ray logs and lithology of well 3 (115m) South-East of study area (right panel).

3 El-Wastani Formation (Quaternary, Early to Middle Pleistocene age)

These Protonile deposits and overly Kafer El Sheikh Formation and underlay Mit Ghamer Formation. It's composed of thick sand beds with thin sand clay beds. The sands sizes are coarse to medium–grained. Some brackish water foraminifera are recorded from few intercalated clay beds. Its maximum thickness is ~300 m. This formation is present with more details at well (1) (Figure 2, left).

4 Kafer El-Sheikh Formation (Tertiary, Early to Middle Pliocene age)

It's composed of clay beds with minor fine sand and silt interbeds. The sand is quartz cemented by clay. The clays are constituted of equal portions of Kaolinite and Montmorillonite with minor Illite minerals. Lower part of this formation is from early Pliocene age and is rich in foraminiferal assemblage. Upper part has a brackish water foraminiferal assemblage. Its maximum thickness is ~1200 m.

Table 1. List of the existing production wells located nearby the study area.

Well Name	Well Depth (m)	Depth to Water Table (m)	TDS (ppm)
W1	121	0.7	29800
W2	100	0.5	29800
W3	122	0.7	33800
W4	113	2.1	25800
W5	116	2.4	29200
W6	108	1.8	32100
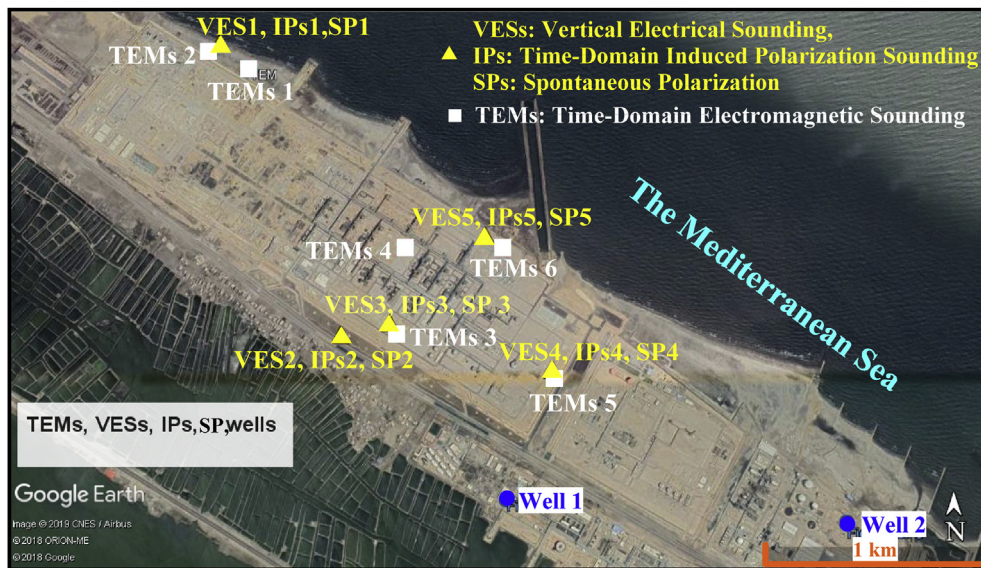
Figure 3. The distribution map of the measured TDEMs, SPs, VESs, and TDIPs with the resistivity and chargeability profiles.
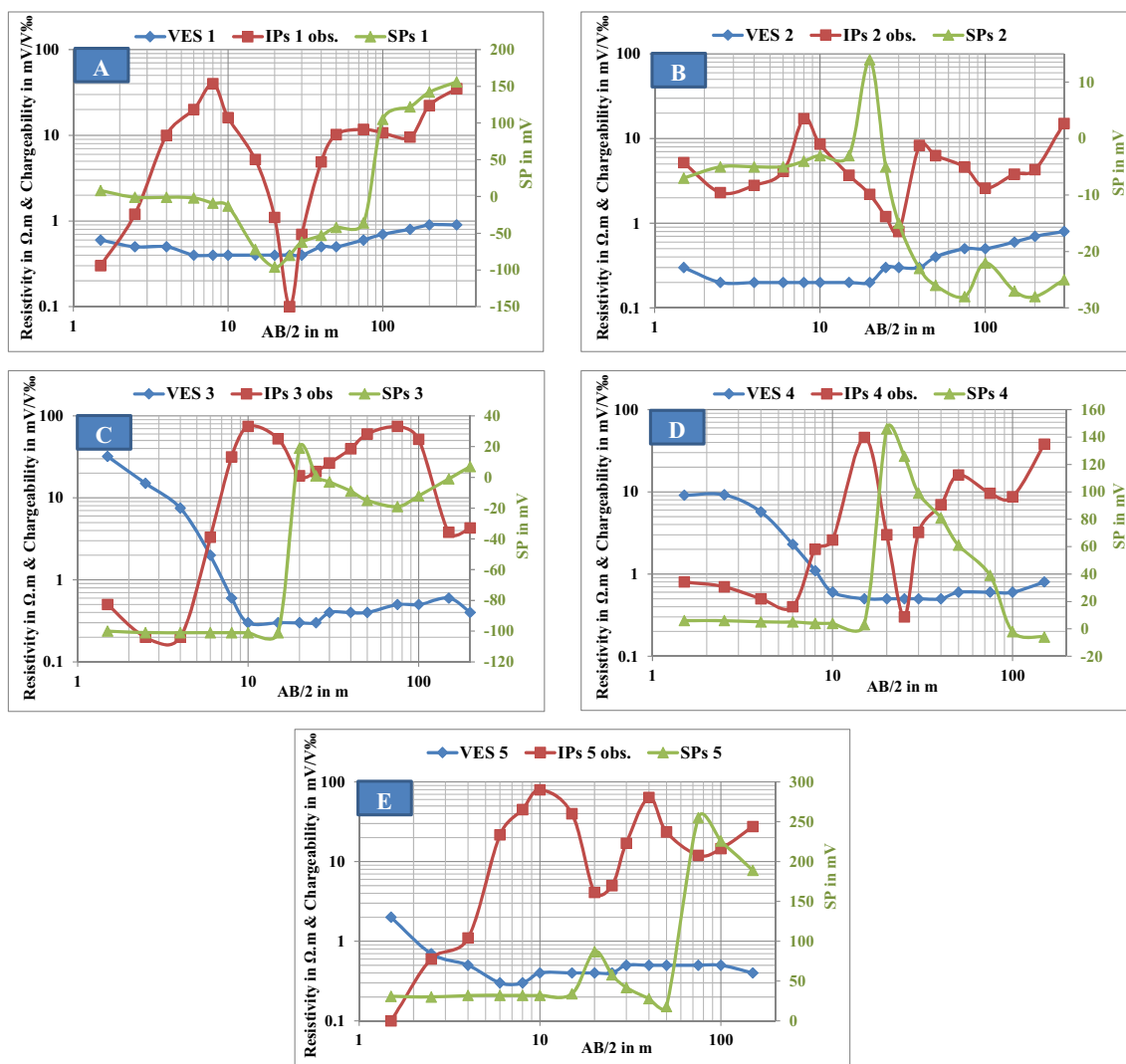
Figure 4. The Resistivity, Chargeability and SP curves of the VESs1, IPs1 and SPs1 (A), VESs2, IPs2 and SPs2 (B), VESs3, IPs3 and SPs3 (C), VESs4, IPs4 and SPs4 (D), and VESs5, IPs5 and SPs5 (E).
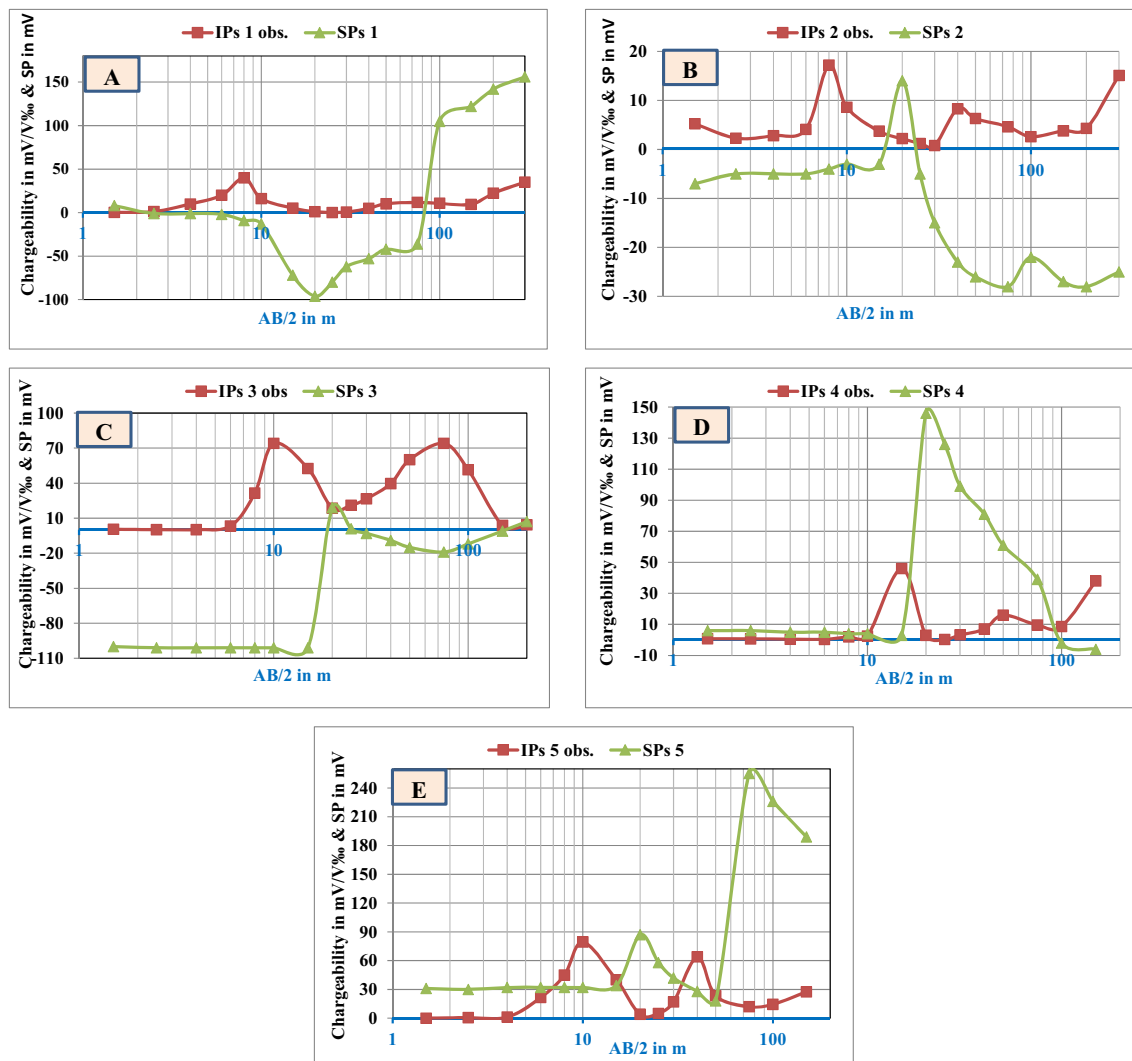
Figure 5. The Chargeability and SP curves of the IPs1 and SPs1 (A), IPs2 and SPs2 (B), IPs3 and SPs3 (C), IPs4 and SPs4 (D), and IPs5 and SPs5 (E).

3. Hydrogeology

Within the study area, there are three different water bearing formations of different importance for groundwater exploitation. Those formations are the coastal deposits, the Sabkha deposits and the Nile flood plain deposits.

3.1. Coastal deposits

These deposits are part of the sea floor and are formed as a result of the tide effect. These deposits consist of very fine sand and clay. It is saturated with brackish/saline groundwater. Hydraulically, it is connected to the Mediterranean Sea. These deposits are under unconfined aquifer condition which is recharged by the direct infiltration from the rainfall. Such deposits exist within the study area near the shoreline.

3.2. Sabkha deposits

These deposits are found mostly in the lowland surrounding Lake Manzala and their thickness is small with no significant groundwater storage. Generally, the sabkhas are characterized by its shallow water table that causes salt accumulation in the formation due to the high evaporation rate. These deposits act as an exit window for the upward groundwater flow in the coastal aquifers.

3.3. Nile flood plain deposits (quaternary aquifer)

These deposits are the most important geologic formation in the study area. These deposits belong to the Nile Quaternary aquifer. The top boundary of these deposits is made up of a semi-pervious clay and silt layer and it acts as a cap for the main Quaternary aquifer. It is generally heterogeneous and anisotropic. These deposits consist of Nile silt, sandy clay, clayey sand, occasionally with fine sand intercalations. The clay content in the topsoil layer ranges between 5% and 50%. However, the silt content varies between 5% and 95%. Due to the low transmissivity and high salinity values of the upper clay layer, this layer is not assumed to be an economically useable aquifer. This layer is of ~25m thick as shown from the well log results of the composite well 3 (Figure 2, right). The water in this layer is in contact with the main underlying aquifer through downward or upward leakage. An extensive irrigation and drainage network break through this layer to serve the agricultural development. The average vertical hydraulic conductivity of the clay cap is 2.5 mm/day, and the average horizontal hydraulic conductivity varies between 50 and 500 mm/day (RIGW, 2018). After a depth of ~30m as shown on well 3, the clay content decreases with depth up to ~102m. This means that the aquifer at these depths is heterogeneous and the hydrogeological properties will be more complex. In central Nile Delta, several pumping tests were performed in the past, which revealed the average hydraulic conductivity to be 1.2×10^{-3} m/s, the average transmissivity to be 10.26 m^2/s, and the average storage coefficient to be
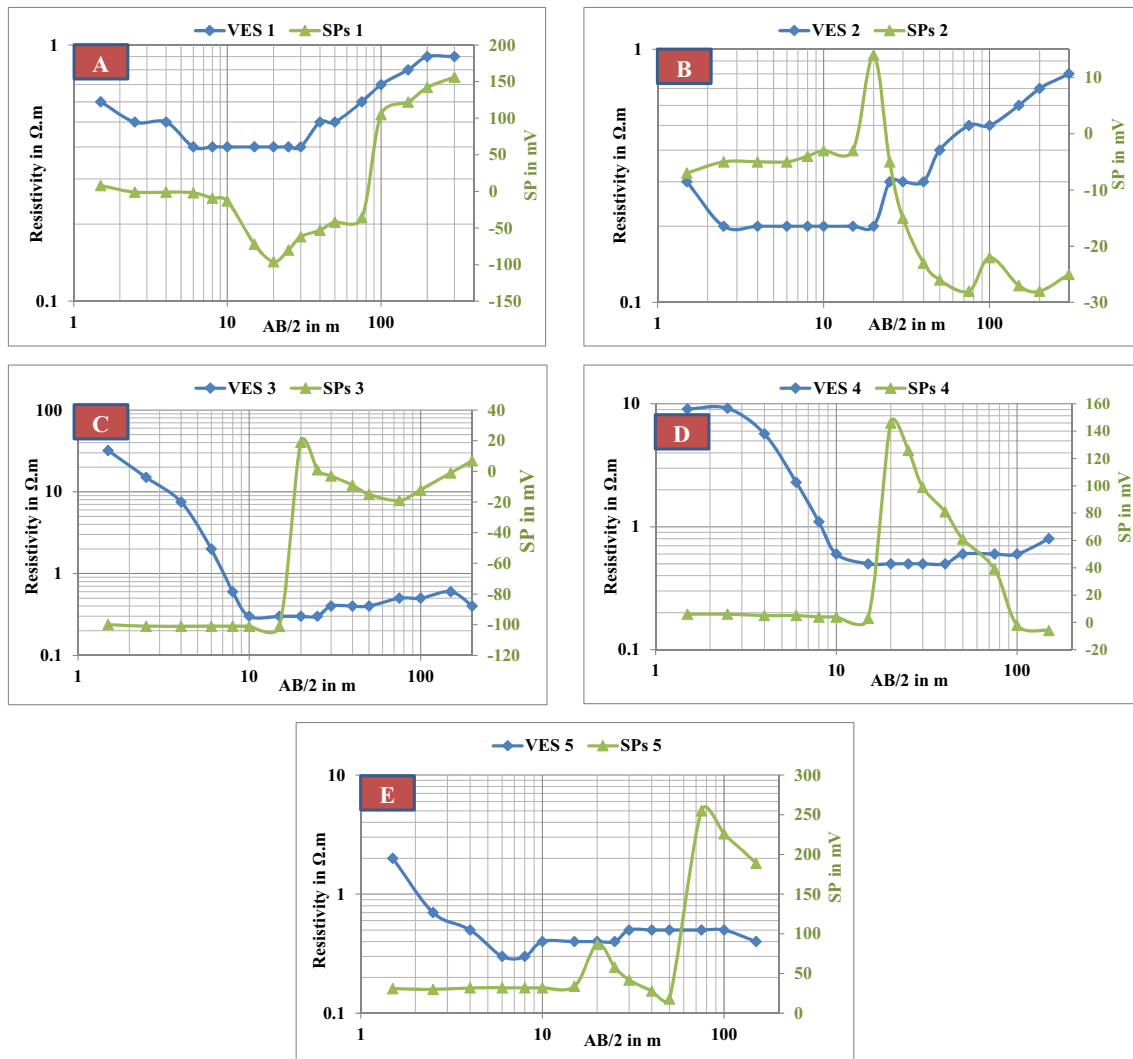
Figure 6. The Resistivity and SP curves of the VESs1 and SPs1 (A), VESs2 and SPs2 (B), VESs3 and SPs3 (C), VESs4 and SPs4 (D), and VESs5 and SPs5 (E).
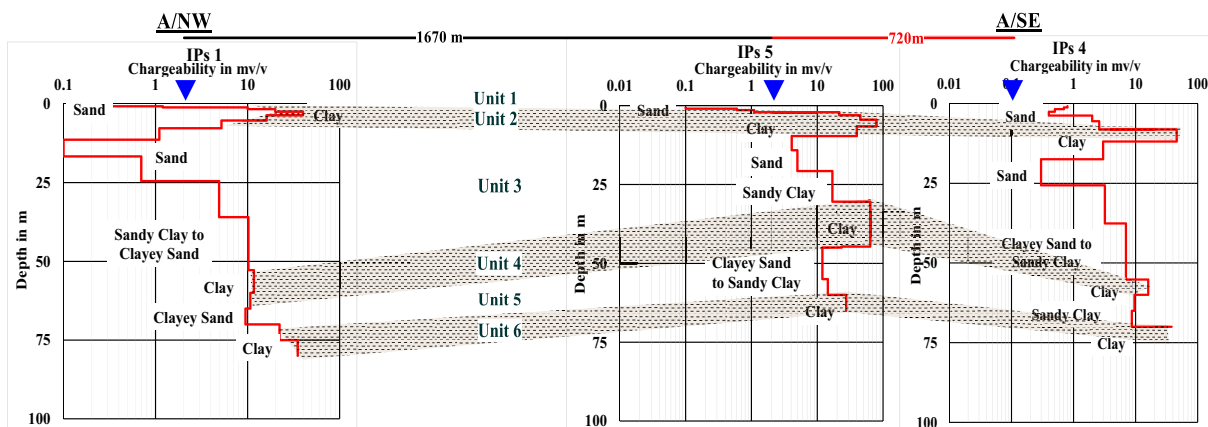
Figure 7. Chargeability profile A-A includes IPs 1, IPs 5 and IPs 4 with the stratigraphic units.

1.5×10^{-4} (Gemail et al., 2017). These values decrease to the north near the coastline in the study area due to increase in clay content.

The main Quaternary aquifer consists of coarse sand and gravel with occasionally clay lenses intercalations. It underlies the top clay layer and overlies the lower marine clay deposits of Neogene impervious clay. The saturated thickness of this aquifer within the study area varies between

800 and 900 m. The aquifer is under semi-confined conditions and the aquifer receives its recharge from the applied irrigation on the surface and the recharge from the irrigation canals. No pumping test analysis was conducted within the study area but the hydraulic conductivity of the Quaternary aquifer varies between 50 and 100 m/day. The aquifer storage coefficient in Delta region varies between 0.20 and 0.0001
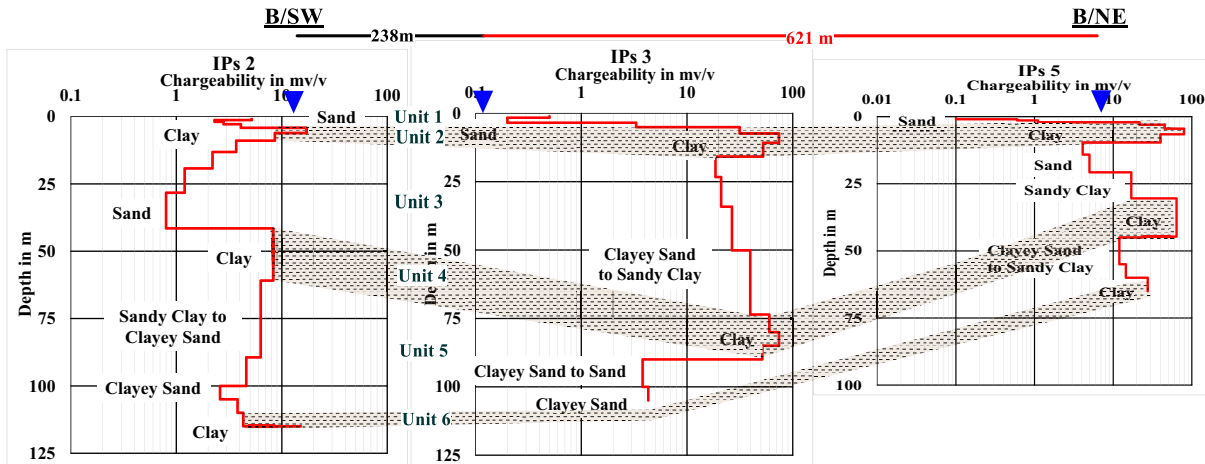
Figure 8. Chargeability profile B–B includes IPs 2, IPs 3 and IPs 5 with the stratigraphic units.
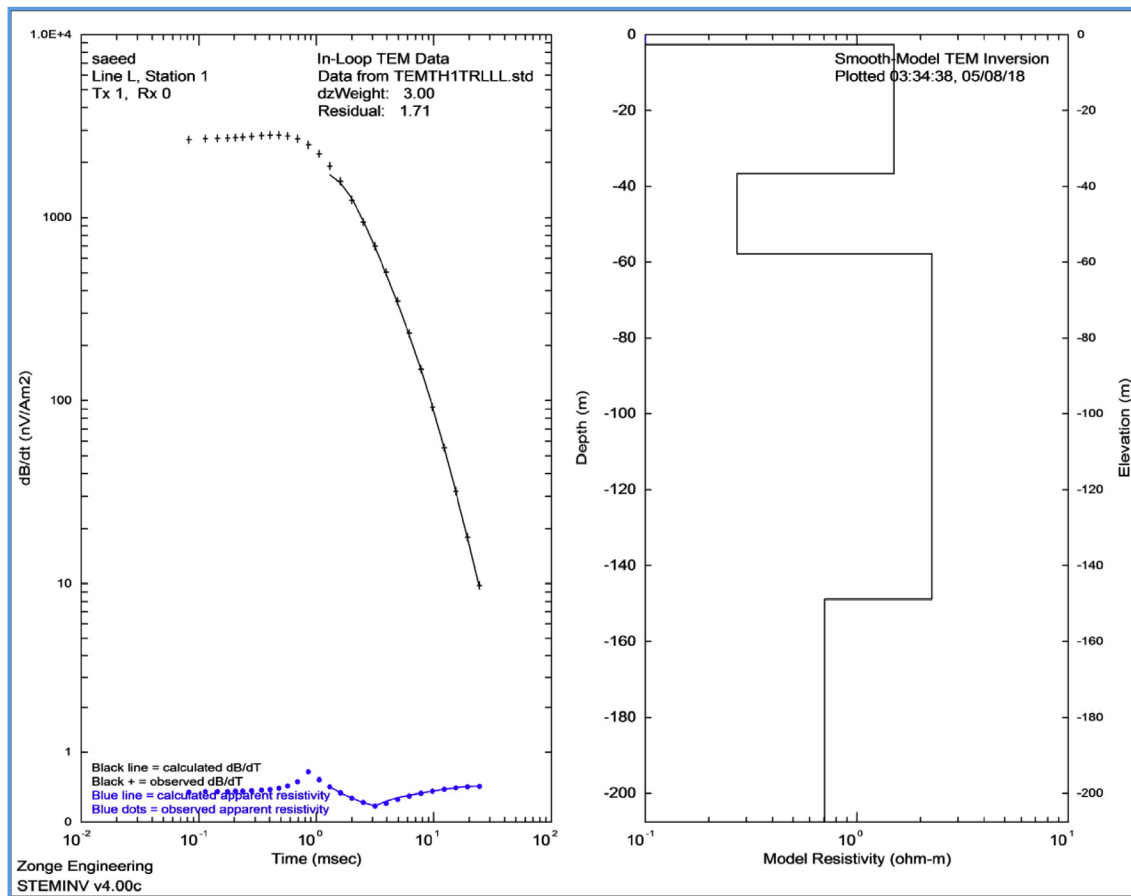
Figure 9. The observed voltage (dB/dt) data (+) and calculated voltage (solid black line) curve vs time (left) and the converted late time observed ρ_a data and calculated ρ_a curve vs time (left/blue), as well as the corresponding geo-electric layers from inversion model in form of resistivity with depth/thickness (right) for TEMs 1.

(RIGW, 2018). The groundwater utilization from such aquifer depends mainly on the water quality and its suitability for the different uses. The Quaternary aquifer is in contact with the Mediterranean Sea which causes the sea water intrusion phenomenon. The depth to the groundwater surface is less than 5 m in most of the Nile Delta region (RIGW, 2002). Within the study area, the depth to groundwater decreases in the north direction. As a result, water logging problems are encountered in such area. Groundwater levels in the Nile Delta aquifer fluctuate in response to the stage of the Nile River, aquifer recharge from excess irrigation water and groundwater pumping. No groundwater extraction from the Quaternary aquifer has been reported, as the groundwater is salty and is not suitable for irrigation or drinking purposes. The well depth reaches up to 120 m (Table 1) with screen length varying between 22 and 60 m. The pumping rate is ~150 m³/hr and the corresponding drawdown is 12m. The Quaternary aquifer in the area is hydraulically connected to the sea water.

From the piezometric head map (RIGW, 2002) of the Quaternary aquifer, the groundwater level decreases towards the north direction with
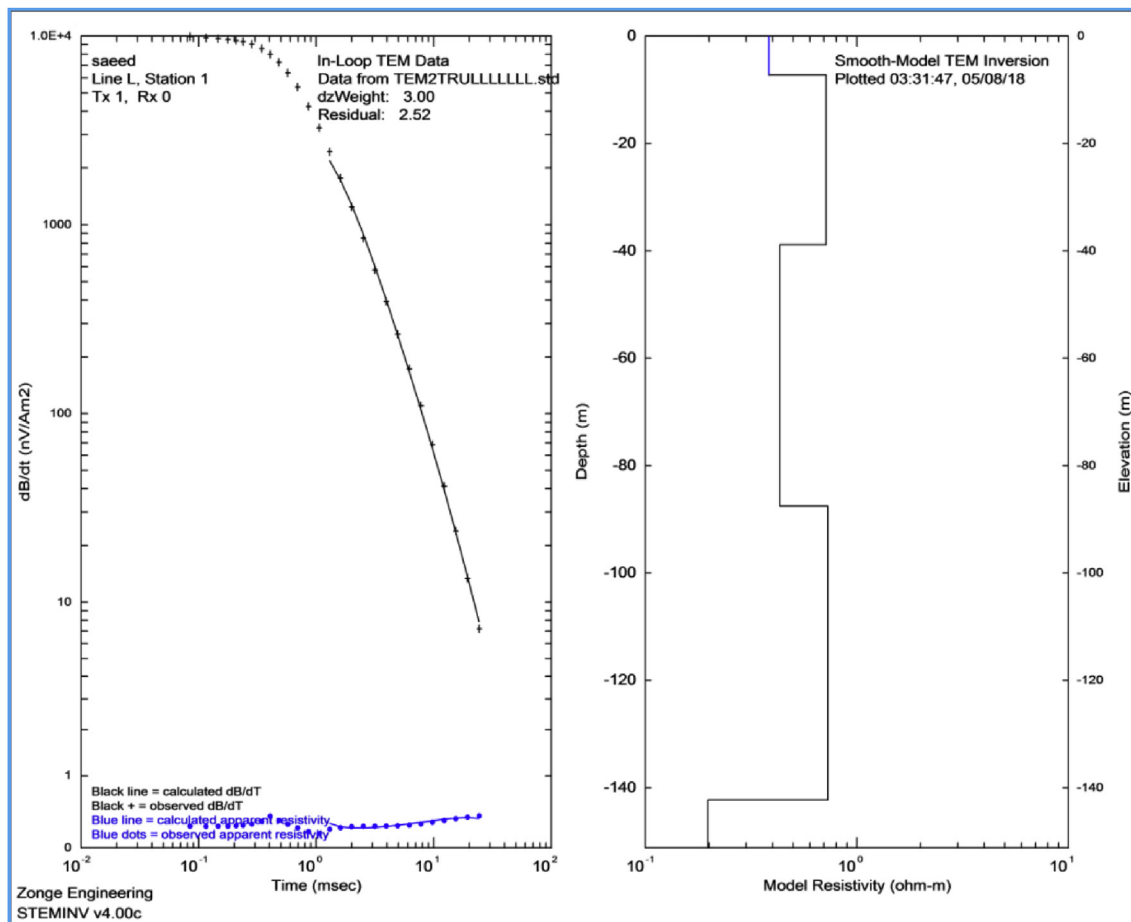
Figure 10. The observed voltage (dB/dt) data (+) and calculated voltage (solid black line) curve vs time (left) and the converted late time observed ρ_a data and calculated ρ_a curve vs time (left/blue), as well as the corresponding geo-electric layers from inversion model in form of resistivity with depth/thickness (right) for TEMs 2.

an average gradient of 11 cm/km. Within the study area, the groundwater head is less than one meter above mean sea level. Due to the industrial nature of the study area, several wells are being drilled recently to provide saline water for the desalination plants. Table (1) shows a collected list of the existing wells located nearby the study area boundaries. The typical well diameter is 280 mm and the designed pumping rate is about 70 m³/h. The total dissolved solids (TDS) vary between 29200 and 35800 ppm. These values will effect intensively on the measured electrical potential from the used geophysical methods. Accordingly, due to the intensive effect of these salinity values, the suitable geophysical method will be chosen for dealing with such conditions and also studying the effect of brine water values on depth of penetration.

3.3.1. Hydro-geochemistry of the Nile Delta aquifer

The groundwater of the Nile Delta aquifer is of meteoric origin. This meteoric water covers the entire Delta except the coastal area, which is occupied by saline water of marine origin coming from either the Mediterranean Sea or from the old marine deep aquifers. Near the coast where the study area, NaCl to seawater type is found, indicating that the groundwater is invaded by the saline water from the Mediterranean Sea or affected by the saline groundwater flowing upward from the deeper aquifers (RIGW, 2018).

3.3.2. Seawater intrusion phenomenon in the Nile Delta aquifer

In coastal aquifers, the general class of groundwater systems consists of a saturated porous medium containing a miscible fluid of variable density. In such systems, the denser saltwater, from sea water intrusion and upward seepage, tends to remain separated from the

overlying freshwater, from rainfall and Nile River. However, a zone of mixing known as the transition zone is formed between the two fluids of different density. The saltwater is not static but flows in a cycle from the floor of the sea to the transition zone and back to the sea. The shape and movement of this zone is governed by the hydrodynamic balance of the fresh water and saltwater. The salinity distribution indicates that the transition zone of brackish water (concentration from 2000 to 10,000 ppm) and saltwater (concentration greater than 10,000 ppm) forms a wedge extending into the aquifer to a distance of 90 km from the coast. Generally, the collected data for showing the salinity distribution along the Mediterranean Sea at different depths revealed that the salinity increases with depth and might reach up to 90,000 ppm at depth of 600 m (RIGW, 2018). In general, the groundwater head of the Quaternary aquifer is less than one meter above sea level. Therefore, the presence of fresh water is restricted to a very small thickness over the salt water. So, the gradual increase in groundwater pumping from the aquifer of Nile Delta leads to less fresh groundwater outflow to the Mediterranean Sea. As a result, the sea water intrusion towards the coastal aquifer increases over time and reduces the availability of fresh water. The available groundwater quality results showed that all groundwater dissolved solids reach the salinity degree of sea water.

4. Geophysical methods

The Spontaneous Polarization Method (SP), the DC Resistivity Method (VES), and the DC Time-Domain Induced Polarization Method (DC-TDIP), as electric methods, and the Time-Domain Electromagnetic
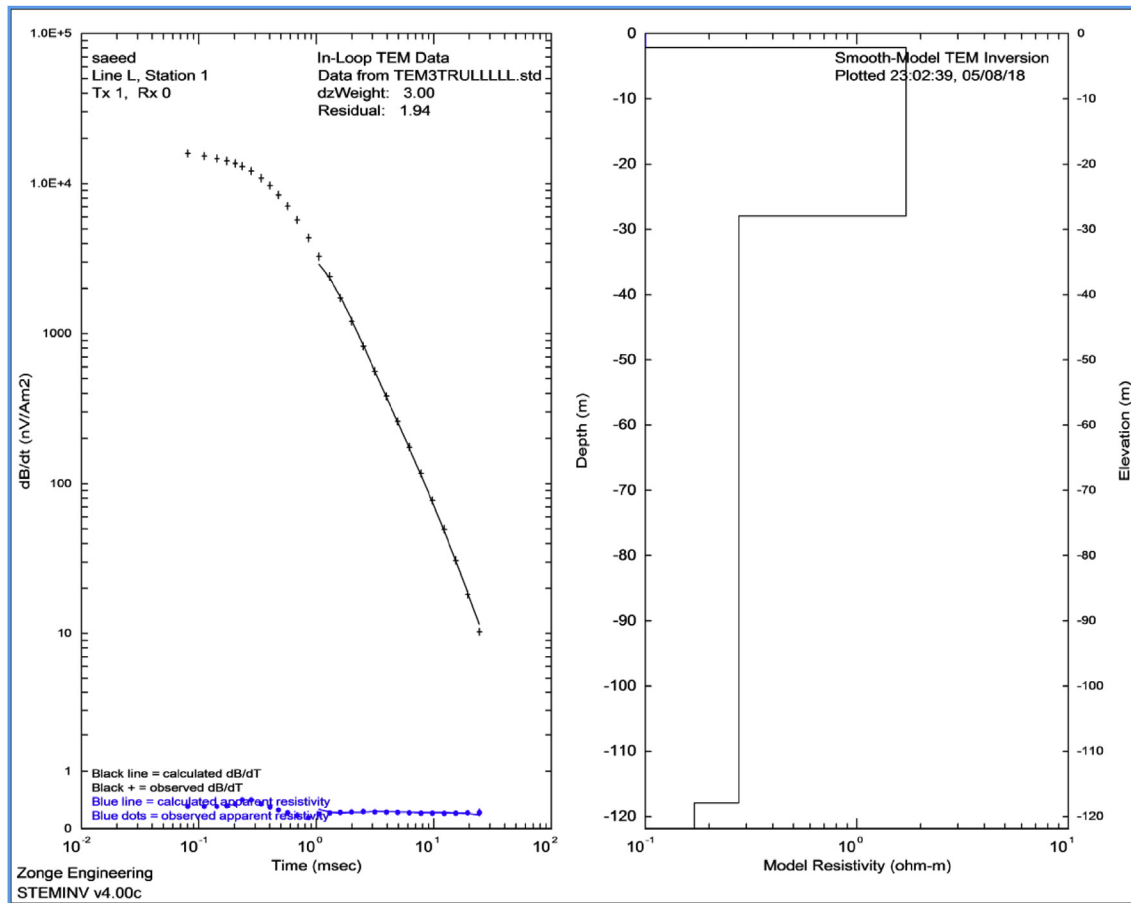
Figure 11. The observed voltage (dB/dt) data (+) and calculated voltage (solid black line) curve vs time (left) and the converted late time observed ρ_a data and calculated ρ_a curve vs time (left/blue), as well as the corresponding geo-electric layers from inversion model in form of resistivity with depth/thickness (right) for TEMs 3.

Method (TDEM), as electromagnetic method, were used in this study, in order to study and compare the geophysical and hydrogeological responses and properties of the coastal aquifer. The possibility of comparing these methods to detect these types of aquifers and their role in differentiation and separation between their different sediments will also be studied. The ability of these methods to penetrate to deep depths will also be studied, with effect of the salt and clay concentrations on the penetration of electric current.

4.1. Electric methods

4.1.1. Data acquisition (instrument and measurements)

The electric methods include the Spontaneous Polarization (SP) method, the DC Resistivity method, and the Time-Domain Induced Polarization method. Generally, field measurements were carried out by using the SYSCAl-R2 resistivity meter and applying the Schlumberger array. The used mode in SYSCAl-R2 to measure resistivity and chargeability was Rho and IP mode. The apparent resistivity data (Ω. m) were measured for 5 vertical electrical soundings (VESs), with a max and min AB/2 ranging from 150 m to 300 m. Also, the spontaneous polarization (mV) of 5 spontaneous polarization soundings (SPs) and the chargeability in mV/V (‰) of 5 Time-Domain induced polarization soundings (TDIPs) were measured using the same previous spacing. Data were distributed on Figure 3 with the distribution of TEMs.

The measured data as curves for apparent resistivity, chargeability and SP are shown in Figure 4. Most of the orientations (azimuth) of these VESs (1, 2, 3, and 5) are parallel to the shore line except for one VES (VES 4) perpendicular to the shore line. The soundings sites selected aim to

distinguish between fresh and brackish water and to separate the different stratigraphic units, i. e. sand and clay of subsurface sediments.

4.1.1.1. Spontaneous Polarization (SP) method. The spontaneous polarization value (in mV) was measured exactly before the electric current is injected into the earth. The SP process is sensitive to the groundwater flow, bulk water chemical composition, and pore water/mineral interface. The fluctuations and signals of SP are utilized to visualize the dissimilarity in ground resistivity prior to the electric current injecting (Revil et al., 2012). Negative values are an indication of an increased of clay content, which is intercalated with other sediments such as sand. The spontaneous polarization method is the result of the natural potentials of electrochemical reactions below the surface. Electric currents are not required to be injected through ground (e.g. resistivity and IP methods). The electrochemical potentials arises between electrolytes of different concentrations and/or composition separated by some chemically active substances such as clay (Gross and Moore, 1959). The current conditions for this potential are the occurrence of clay-sand contacts and brine water. It differs from the IP method which is used to distinguish between clay and non-clay strata. Groundwater is an important factor for SP. The potentials are produced by the flow of water. Water reacts as a solvent and an electrolyte for various minerals. Porous rocks electrical conductivity depends on several factors such as the porosity and the mobility of charged ions through the pore spaces.

Figure 5 shows a mirror image comparison between SP (low) and IP (high) for clay or clayey sediments and the reverse between SP (high) and IP (low) for non-clay sediments. Also, the same condition is present in the SP and resistivity measurements (Figure 6), but due to the increased
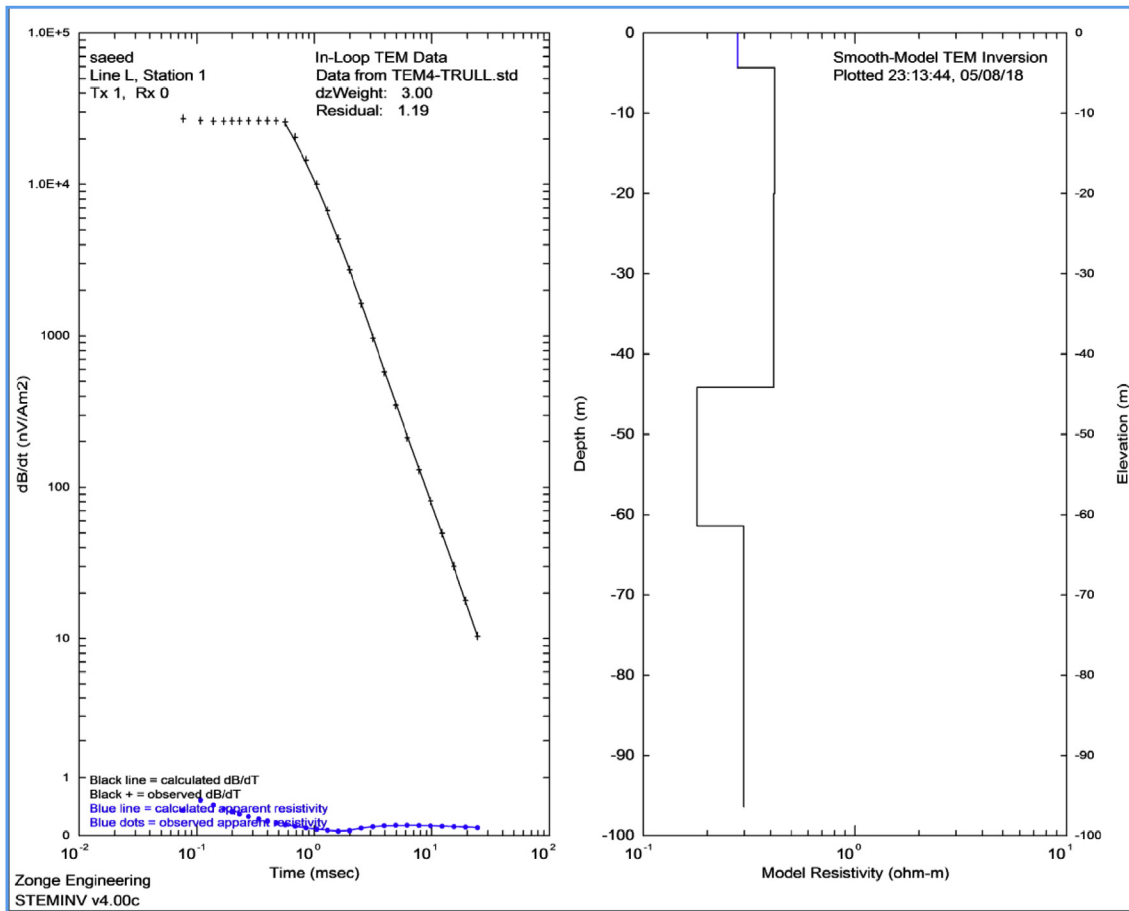
Figure 12. The observed voltage (dB/dt) data (+) and calculated voltage (solid black line) curve vs time (left) and the converted late time observed ρ_a data and calculated ρ_a curve vs time (left/blue), as well as the corresponding geo-electric layers from inversion model in form of resistivity with depth/thickness (right) for TEMs 4.

salinity and concentration of clay, the resistivity values are more difficult compared to SP and IP.

4.1.1.2. DC resistivity method. The main objective of the resistivity method is for measuring the apparent resistivity of subsurface materials in the form of apparent resistivity curves (Figure 4). These curves show the increasing salinity of water and clay with silt being the two main materials that affected the decrease in resistivity values. Qualitatively, these curves have been interpreted and shown that the sediments are filled with highly saline water and the different sediments cannot be separated. Therefore, these values will lead to some unclear validation between water of different salinity and clay or clayey sediments. So, we have to find some other methods of differentiation.

4.1.1.3. Time-Domain Induced Polarization (TDIP) method. The TDIP (DC-IP) process measures decay of voltage induced by turn-off of excited current oscillation and uses the decay response characteristics to study the induced polarization (chargeability) of the soil. Induced Polarization measures the polarization ability of soil when influenced by the electric field; during polarization process there is an inverse energy in the soil (Marshall and Madden, 1959). Time-Domain IP (TDIP) surveys are loaded by sending current into ground and the potential difference is measured to determine the resistivity. When the current is turned off, the potential decay at ground is measured again at one or several time intervals windows. A common parameter used to define TDIP measurements is chargeability, which is defined as the ratio of the secondary potential over the primary potential of the transmitted current. To measure the secondary potential, a separated integration is used to log

the potential data logarithmically into the time gate spaces. Time-gate spaces and the duration of the current pulses on and off times are effective on the magnitude of the chargeability integral (Seigel, 1959; Magnusson et al., 2010; Sumner, 2012). Therefore, it is not easy to make a comparison of the different methods. Resistivity is a parameter dependent on bulk; integral chargeability is dependent on settings of measurements.

Immediately after turning on of the current, the induced potential, V_i, rises across the potential electrodes. After the charging-up effect, the primary voltage, V_{DC}, is measured to calculate the DC resistivity before the current is turned off. At turn off of current, the voltage drops to the secondary level, Vs, and the voltage decays with time (relaxation time). This decay curve is the target of the time-domain IP method, as it is a characteristic of a material according to the premier magnitude, slope and relaxation time. The signal V_{ip} along the decay is usually integrated over n time windows, or gates to calculate the chargeability M. The discharge phenomenon observed during the relaxation time.

A high voltage was sent to the earth to overcome the effect of highly saline water on the main chargeability of the sediments. The measured chargeability, which is computed from the formula (1), is Raw and it considered as Normal because the used period was 2000 ms and it is expressed as (Schön, 2015; Slater and Lesmes, 2002):

$$M_i = \frac{i}{V_{DC}[t_{i+1} - t_i]} \int_{t_i}^{t_{i+1}} V_{ip} dt \tag{1}$$

Where: V_{DC} [V] potential used to calculate DC resistivity, V_{ip} is the intrinsic or secondary potential [mV], and t_i and t_{i+1} are the open and close times [s] for the gate over which signal is integrated.
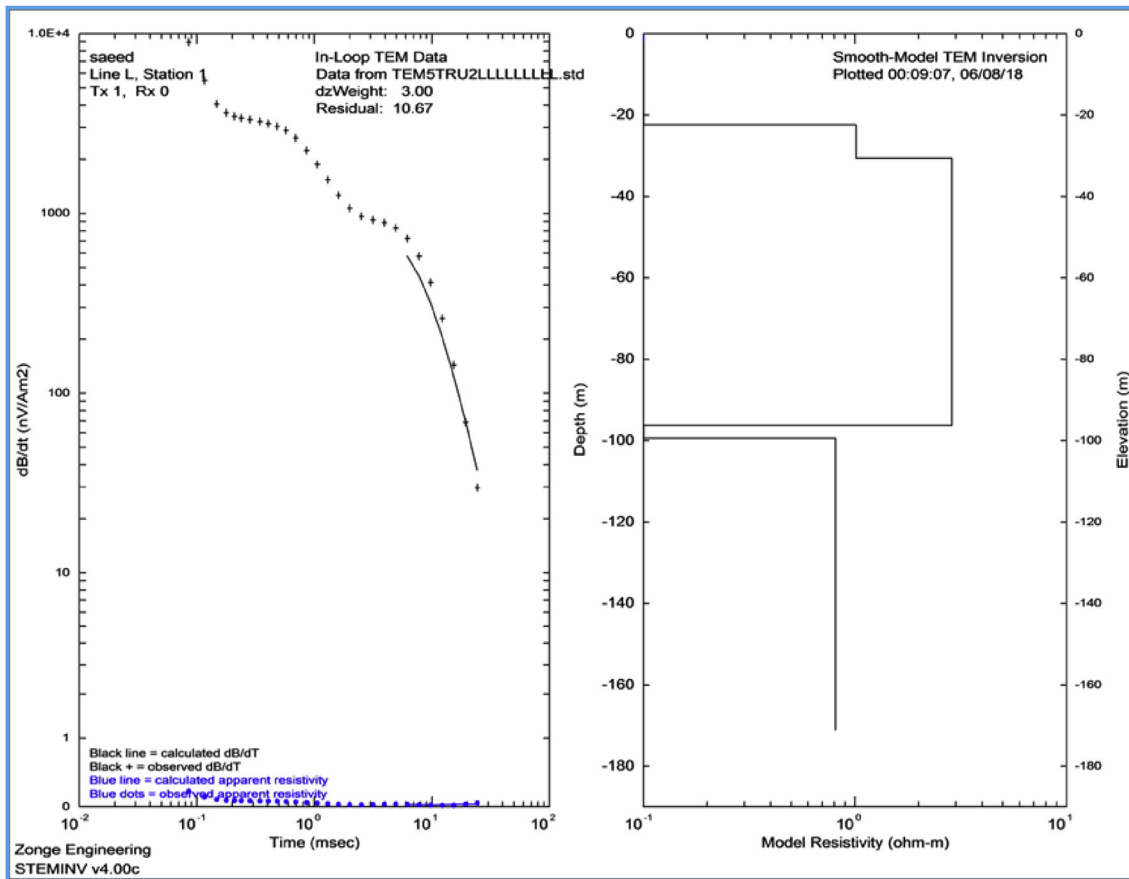
Figure 13. The observed voltage (dB/dt) data (+) and calculated voltage (solid black line) curve vs time (left) and the converted late time observed ρ_a data and calculated ρ_a curve vs time (left/blue), as well as the corresponding geo-electric layers from inversion model in form of resistivity with depth/thickness (right) for TEMs 5.

The partial chargeabilities measurements (Mi) and the weighted average global chargeability deduced (M) give some information regarding the capacity of the soil to charge due to current flow. Partial chargeability of the window (i) is computed from the formula 2 as following:

$$Mi = \int_{T\_Mi} Vdt / T\_Mi.V_{MN} \qquad (2)$$

And the global chargeability is computed from the formula 3 as following:

$$M = \sum_{i=1}^{n} (Mi. \, T\_Mi) \bigg/ \sum_{i=1}^{n} T\_Mi \qquad (3)$$

Where: M average value of global chargeability (mV/V) (‰), M_i average value of partial chargeability (i) (mV/V) (‰), n is the number of IP windows, and T_Mi is the width of partial chargeability window (i).

4.1.1.3.1. IP data processing and inversion. Due to the occurrence of polarization process, the IP interpretation for geological subsurface layers is complicated by the heterogeneity of soils and rocks. Moreover, the difficulty of the polarization technique arises from several factors such as mineral structure, chemical environment, and texture adding to many other factors (Revil and Florsch, 2010; Weller et al., 2013; Revil et al., 2015). Therefore, sediments with high clay content have high chargeability values. Also, soils with uniform sand and gravel particle size produce lower chargeability (Alabi et al., 2010). The variance of normalized chargeability determines the potential permeable rocks that can contain or transport groundwater from clean clay sediments. Therefore, the observed and calculated values of chargeability with

depth were used for all TDIPs to separate the clay and non-clayey sediments.

4.1.1.3.2. IP profiles and results. Two chargeability profiles, A-A profile, NW-SE direction and B–B profile, W-E direction (Figures 7 and 8) are designed. In profiles A-A and B–B, the minimum and maximum depths of measured chargeability were 45 m and 90 m, respectively. The measured chargeability in this area was used for separating the clayey and clean sediments from sandy sediments. Interpretations of Vertical Electrical Sounding (VESs) of subsurface resistivity in highly saline coastal sediments are complex and difficult due to the effect of high salinity (Figure 4).

TDIP method is more stringent in separating thin clay layers than the TEM method, especially, at depths up to 90 m (Shallow depths). Accordingly, the recorded stratigraphic units were interpreted as six (Figures 7 and 8) and their chargeability values and geological properties are:

➢ **Unit 1** with low chargeability is sand, and its thickness ranges between ~1 m and ~3 m.
➢ **Unit 2** with medium to high chargeability is clayey sand to sandy clay to pure clay with thickness ranging from ~3 m to ~4 m.
➢ **Unit 3** with low to medium chargeability is sand to clayey sand to sandy clay with thicknesses between ~4 m and ~8 m.
➢ **Unit 4** with medium to high chargeability is clayey sand to pure clay with thicknesses ranging from ~7 m to ~17 m.
➢ **Unit 5** with low to medium chargeability is sand to sandy clay with thicknesses from ~10 m to ~45 m
➢ **Unit 6** with medium to high chargeability is clay with thicknesses ranging from ~30 m to ~70 m and sometimes around ~90 m.
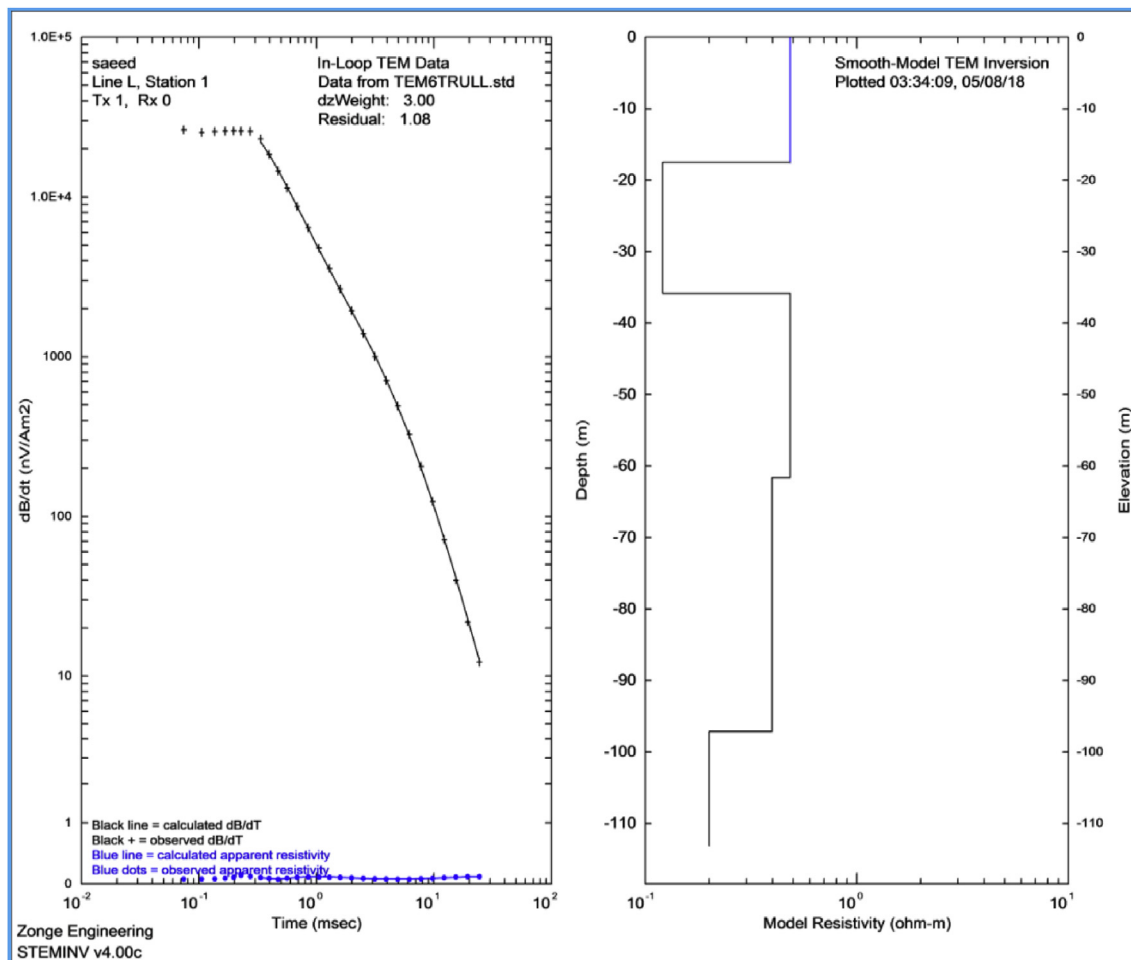
Figure 14. The observed voltage (dB/dt) data (+) and calculated voltage (solid black line) curve vs time (left) and the converted late time observed ρ_a data and calculated ρ_a curve vs time (left/blue), as well as the corresponding geo-electric layers from inversion model in form of resistivity with depth/thickness (right) for TEMs 6.

4.2. Electromagnetic method

4.2.1. Time-domain (transient) electromagnetic method

Electromagnetic (EM) is the primary method used in hydrogeological inspections due to its ability to distinguish between formations of different resistivities (Goldman and Neubauer 1994). Transient electromagnetic soundings (TEMs) were used without restriction to map changes in groundwater quality, which are dependent on the variation in conductivity (Stewart and Gay, 1986; Kruse et al., 1998). TEMs can be used to map the extension of saltwater intrusion especially in depth estimation and determination of the transition of saltwater zone due to their ability to detect the conductive layers (e.g. salt water or clay) (McNeill, 1990; Kontar and Ozorovich, 2006; Goldman and Kafri, 2006; Shah et al., 2007). TEM method is effective for dry areas. TEM method can explore subsurface depths of up to hundred meters (Fitterman and Deszz-Pan, 1998).

The fundamentals of TEM theory are restricted to the homogeneous half-space model (Kamenetsky, 1997; Kontar and Ozorovich, 2006). In general, TEM uses transient electromagnetic field diffusion under time-domain control (Stewart and Gay, 1986; McNeill 1990, 1994). The current is alternatively turned on and off in a rectangle. A square loop of wire is placed as the transmitter (Tx) source on the ground. The primary (static) magnetic field, perpendicular to the plane of transmitter loop will be produced at turn-on time. During turn-off time, the induced electromotive forces are initiated at ground due to the decay of primary field. This produces some eddy currents at conductive depths. These induced currents penetrate into ground and create a secondary magnetic field with an amplitude that decreases with time. This is measured by a receiver (antenna) coil (Rx) at several predefined times during the turn-off period. The decay shape reflects the distribution of resistivity with depth. By increasing the period of decay voltage, it is possible to obtain some information about the lower distal layers. TEMs use different transmitter or receiver arrangements. The central loop configuration is the most common. This configuration was used in this study and has the receiver at the center of the loop transmitter. Due to the relatively low sensitivity of this method to near-surface inhomogeneity and near-surface layers, SP, DC-Resistivity, and TDIP methods were used. Therefore, the TDEM method will be less ambiguous (Goldman et al., 1989; McNeill 1990).

The transmitter/receiver separation is not effective in exploration depth of the TDEM method (i.e. the separation of TDEM plays the same role as the transmitter current). It is mainly increases the signal-to-noise ratio. The exploration depth determined by the time after transmitter current is turned off. To explore greater depths, it is necessary to record the signal at late times. Indeed, at early time, due to the skin-effect, the induced currents are concentrated in the upper layers. Thus, early measurements of the EM field induced by these currents would be sensitive to the electrical conductivity of shallow structures. With increasing time, the maximum current density will travel to greater depths and the measured signal will depend more on the conductivity of the deeper layers. Moreover, the current density decreases in the near-surface layers and, as a result, the near-surface electrical conductivity structures do not
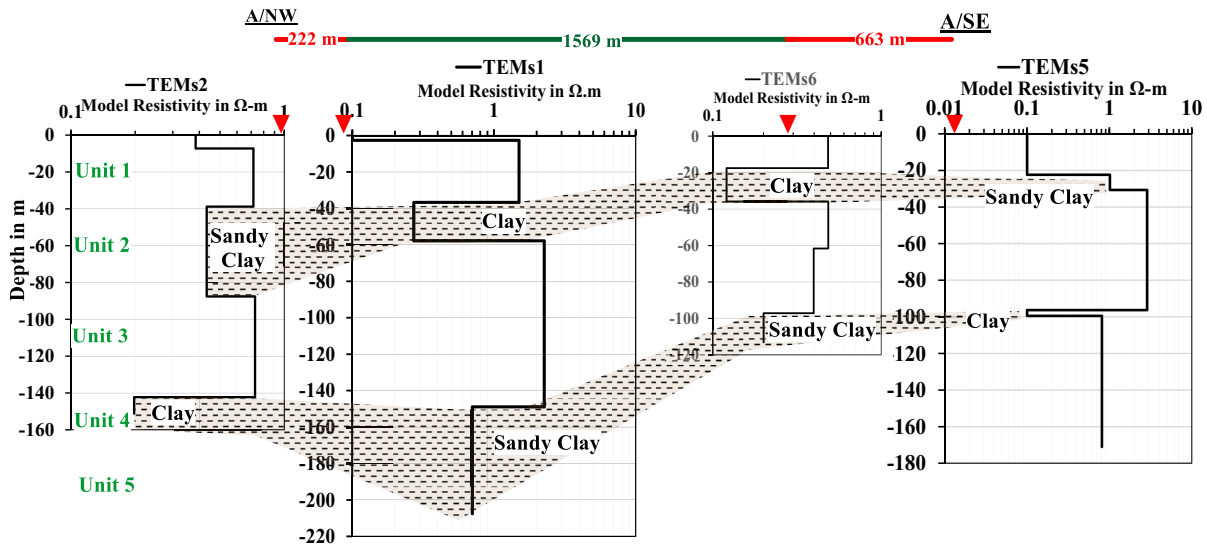
Figure 15. Geo-electric profile A-A from the TEM method includes TEMs 2, TEMs 1, TEMs 6 and TEMs 5 with the stratigraphic units.
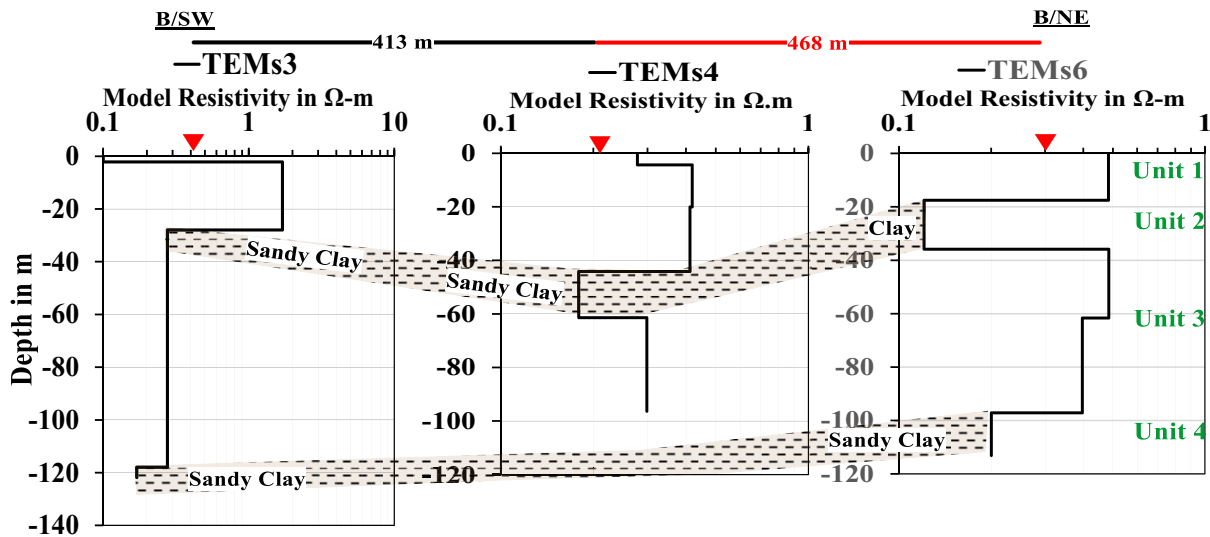
Figure 16. Geoelectrical profile B–B from the TEM method includes TEMs3, TEMs4 and TEMs6 with the stratigraphic units.

affect the measured signal at late times as has been reported in all measured TEMs. This helps to eliminate the effect of near-surface inhomogeneities. The maximum depth of penetration was shallow for two reasons; 1) impact of high conductive surface layer; 2) highly conductive subsurface layers consisting of clay, clayey sediments with high saline water. The second reason complicates the case of penetration of the induced current at the calculated or required depths. Therefore, for these reasons, the maximum penetration depth ranged from 120 to 210 m.

4.2.2. TEM data acquisition (instrument and measurements)

TEM survey conducted with the Zonge GDP-32[24] system, the Geophysical Data Processor (GDP-32[24]) is a universal multi-channel receiver designed to acquire virtually any type of electromagnetic or electrical data from DC to 8 kHz bandwidth with the ZT-30 transmitter. In the TEM transmitter, the ZT-30 can deliver up to 30 A to a 100 m loop with a turn-off time of less than 200 µs. The XMT-G controls the transmitter and makes timing with the receiver accurate to a fraction of a microsecond. The ZT-30 transmitter may operate at 20 A which is safer than 30 A. The transmitter current is controlled by Ohm's law ($I = V / R$); V main power voltage from external batteries; R resistance of loop measured with multi-meter. The ramp time measured by the transmitter

itself. Also, with the XMT-G is a GPS-locked controller for Zonge transmitters. GPS satellites provide highly precise time date with the help of location. This allows the XMT-G to synchronize with the similarly equipped GDP-32 (G) at a remote location without the use of a synchronization cable (possibly kilometers long).

In this study, using a rectangle transmitter loop with different lengths of sides and sometimes of 2 or 3 turns (as in TEMs 6 and 4), respectively. The receiver at the center of transmitter loop (in-loop configuration) measures the electromagnetic fields and the injected current of different Ambers. The higher current at the loop increases the electromagnetic field strength. This increases the precision of the results relating to the deeper layers. The receiver measures the voltage induced from the secondary magnetic field and will be positioned at the center of the loop transmitter. Six (6) TEM soundings are located in two profiles (Figure 3).

The measured data are the values of the receiver output voltage at consecutive time gates. Gates are selected from a few microseconds to hundreds of milli-seconds, after turn-off of the transmitter current, according to the desired penetration depth. The receiving coil (antenna) measures the rate of magnetic field time change e (t) = dB/dt in Nano-Volts per square meter (NV/m^2). Measuring the decay range is from many thousands of nV/m^2 in early times to <0.1 (nV/m^2) in later times
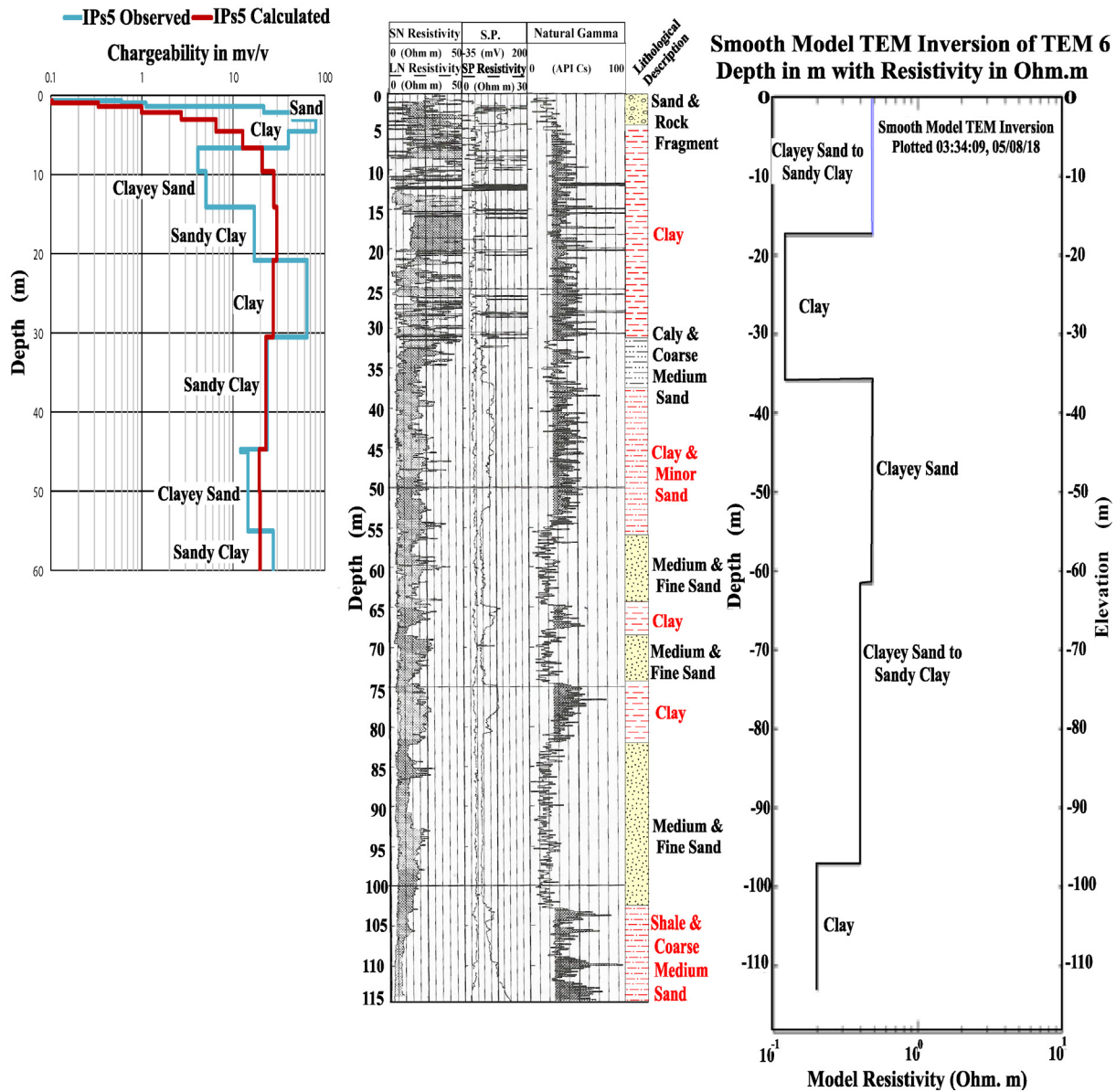
Figure 17. The correlation between the TEM6 (right panel), IP5 (left panel) and the composite log includes short and long resistivity, single resistivity, SP and gamma ray logs of well 3 (middle panel).

(Everett and Meju 2005). Figures 9, 10, 11, 12, 13, and 14 illustrate the measured magnetic field decay (dB/dt) at the selected TEMs. Decay is recorded over 3 decades during the recording channel from 0.1 to 30 ms (TEMs 1). Also, the plots in Figures 9, 10, 11, 12, 13, and 14 show the same data that has transformed into apparent resistivity (ρ_a) in the late-stage. The ρ_a observed and ρ_a calculated curves give the initial pre-diction about subsurface succession. Most TEM soundings use late stage apparent resistivity (McNeill, 1994) and early stage earth resistivity will not be used because it is incorrect.

Using 1 D-layered models with *Zonge engineering* Apparent Resistivity in Ω.m, ρ_a, late time is calculated from the Eq. (4) as following:

$$\rho_a = \left(\frac{IA_T A_R}{V}\right)^{2/3}\left(\frac{1}{T}\right)^{5/3} \times 6.3219E - 3 \tag{4}$$

Diffusion depth d (m) is calculated from the Eq. (5) as following:

$$d = 40\sqrt{\frac{t}{\sigma}} = 40\sqrt{\rho_a t} \tag{5}$$

Equivalent investigation depth D (m) is calculated from the Eq. (6) as following:

$$D = 28\sqrt{\frac{t}{\sigma}} = 28\sqrt{\rho_a t} \tag{6}$$

Where: AT = transmitter moment (m^2), AR = Receiver moment (m^2), I = Transmitter current (ampere), t = Time in msec. V=Received voltage in μV, σ = 1/ρ = Conductivity in S/m.

4.2.3. Processing and inversion of TEM data

All TEM soundings are explained as 1D-layered models using *Zonge engineering, STEMINV v4.00c*. The first involves a user-defined multi-layers model according to the sounding curve as a starting model and uses a forward-modeling algorithm that produces the best-fit solution and which provides many equivalent solutions (Figures 9, 10, 11, 12, 13, and 14). Based on the initial starting and the forward model, the inversion program attempts to find a better fit of the observed data using iterations, to arrive at a very small Root-Mean-Square (RMS%). Data points
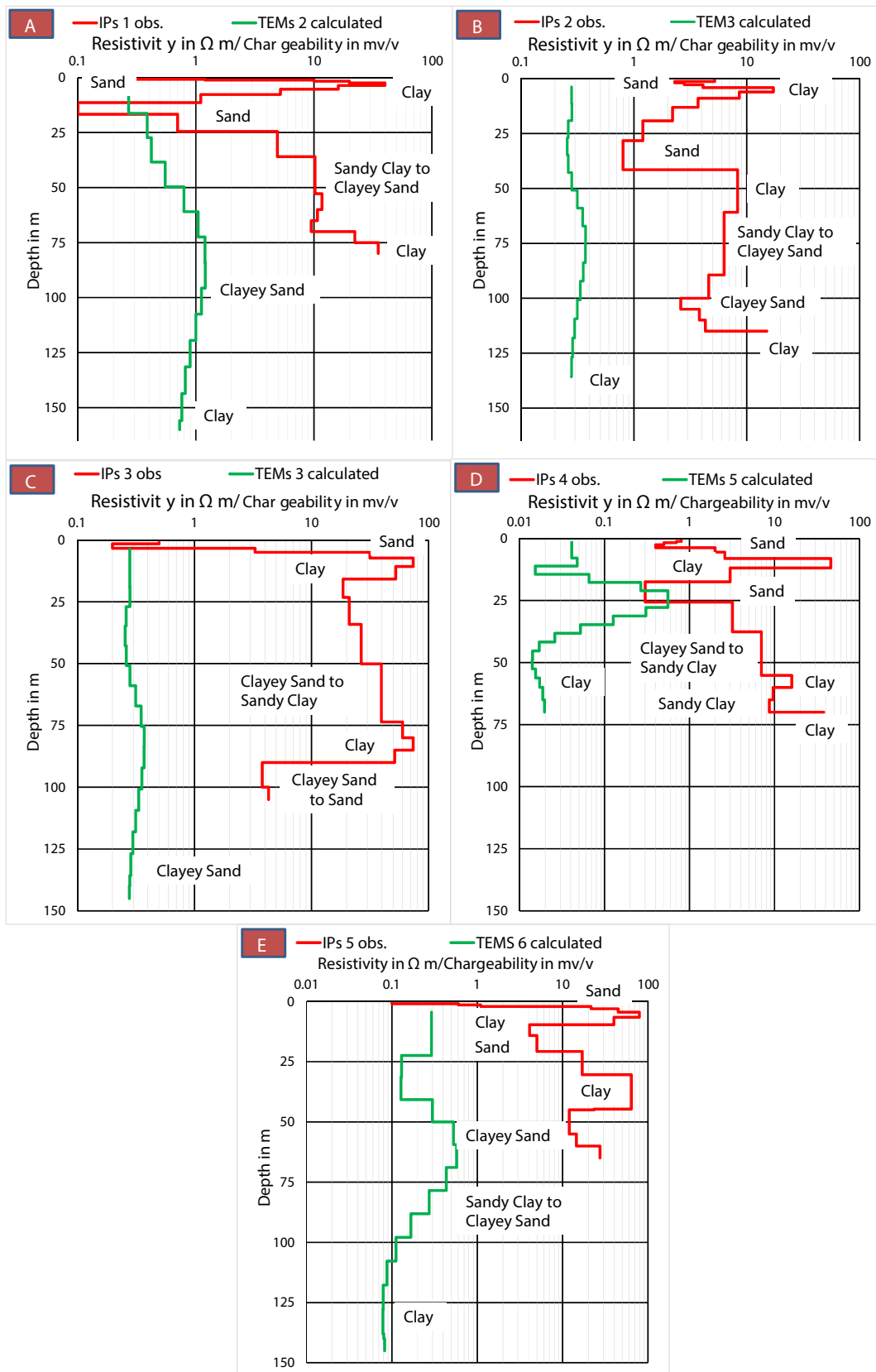
Figure 18. Matching between TDIPs and TEMs with the stratigraphic units for the IPs 1 and TEMs 2 (A), IPs 2 and TEMs 3 (B), IPs 3 and TEMs 3 (C), IPs 4 and TEMs 5 (D), IPs 5 and TEMs 6 (E).
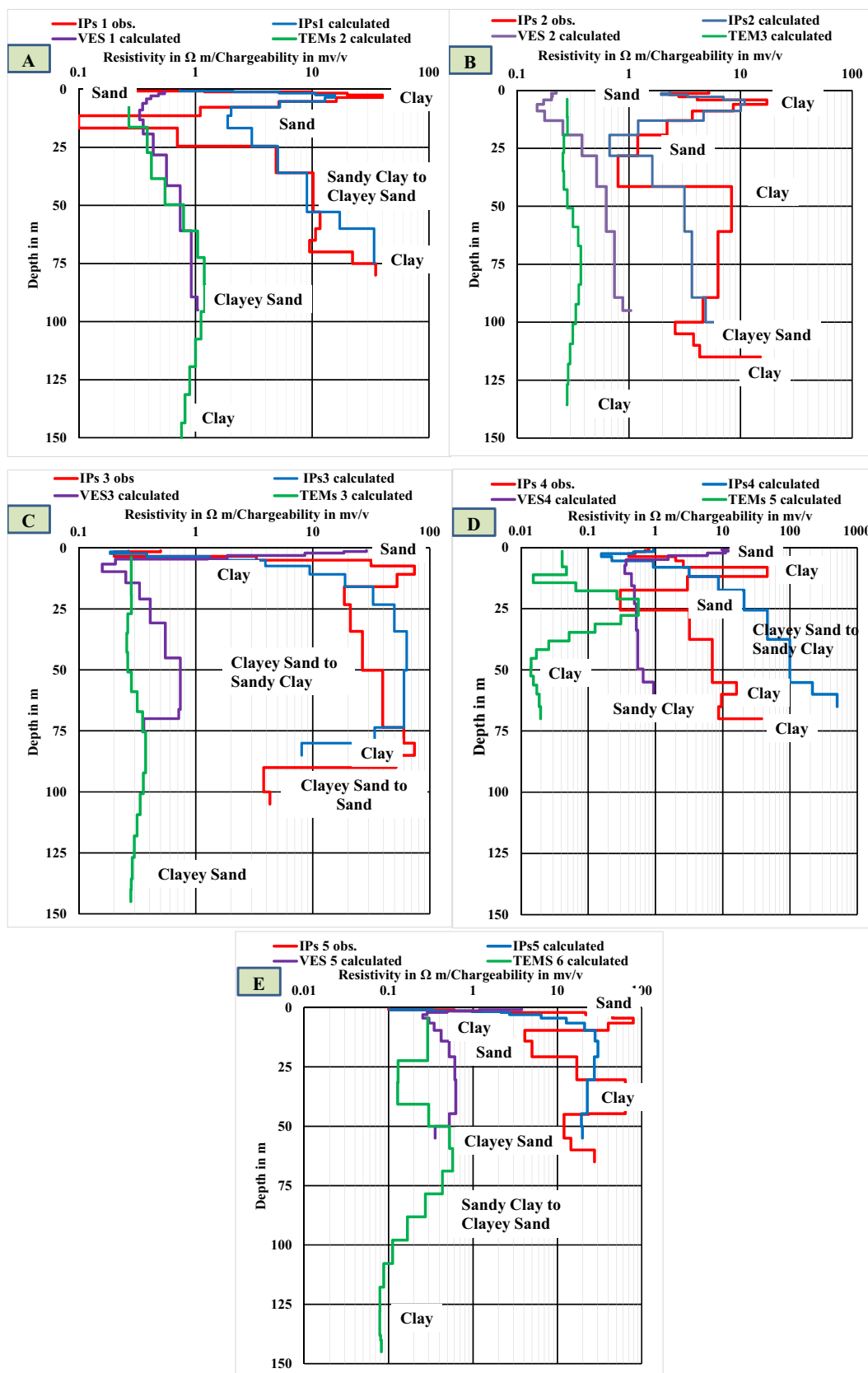
Figure 19. Matching between TDIPs, DC Resistivity, and TEMs with the stratigraphic units for the IPs 1, VES 1 and TEMs 2 (A), IPs 2, VES 2 and TEMs 3 (B), IPs 3, VES 3 and TEMs 3 (C), IPs 4, VES 4 and TEMs 5 (D), IPs 5, VES 5 and TEMs 6 (E).
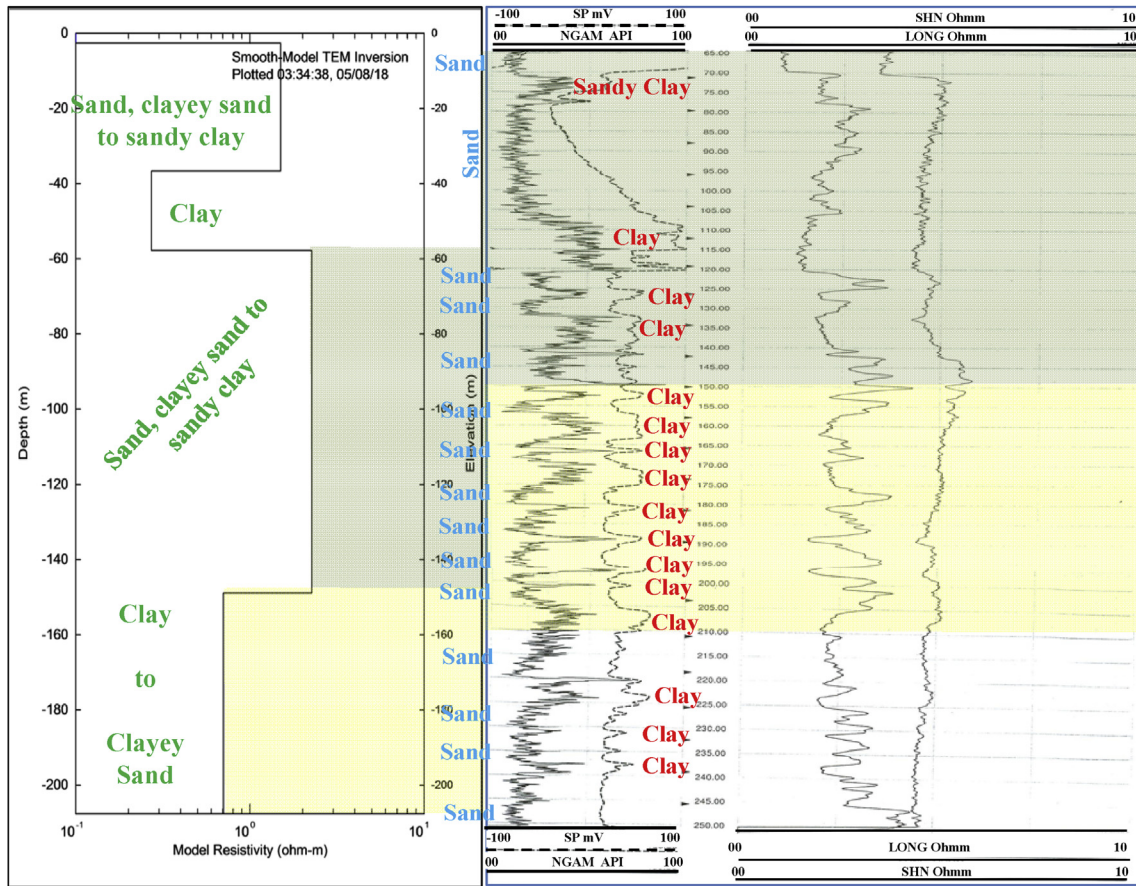
Figure 20. The matching between Deep TEMs1 (left panel) with the composite log (short and long resistivity, SP and gamma ray logs) well (right panel) at same location of TEMs5.

are used to calculate fitting error. The right panel of Figures 9, 10, 11, 12, 13, and 14 shows the geoelectric layers model used to calculate the model response represented as a solid line at the left panel. This layered model represents the vertical delineation of the calculated ρ_a which is a non-unique estimate of the true resistivity of subsurface geological layers.

The smoothing model of resistivity with depth used some iterations with inversion software to find a good fit to the sites. Multiple-iteration inversions were computed until the RMS% between the observed ρ_a and the calculated ρ_a reached an acceptable limit (from 5-10%). The RMS residuals (errors) between the measured ρ_a and the calculated ρ_a for all measured TEM soundings were 1.08%–2.52% excluding TEMs 5, and the RMS% was 10.67% due to the presence of an electrical power source, shallow sand and clayey sand aquifer appearing in the upper part (wavy part) of voltage curve (Figure 13).

4.2.4. TEM results and profiles

After performing an inversion of each TEM sounding, the smooth (1D) model of TEM (resistivity with depth) was imported into one profile. Along this profile all 1D models of TEMs were compared with each other as shown in profiles A-A, NW-SE orientation (Figure 15), and B–B, W-E orientation (Figure 16). Previous TEM profiles show that in profiles A-A and B–B, the minimum and maximum penetration depths were 120 m and 210 m, respectively. Also, the recorded high salinity sedimentary layers are very complex in their stratigraphic units. This shallow penetration is due to the TEM method is very sensitive to the conductive layers and has low sensitive to the resistive layers. Due to the large amount of current flows in the conducting layers, this method is very sensitive to it. Along the study area, the depth to water (highly saline water) is close to the surface (<1.5). Therefore, the diffusion speed of current with depth

will be low due to very low-resistive layer after 0.5–1.5m along the study area.

Also, this method is evident in the low sensitivity of the layers near the surface and the presence of in-homogeneities near the surface. The thickness of the low-sensitivity surface layer (not recorded layer) was small because the depth of the high salinity water table was close to the surface (from 0.5-2m).

In comparison between TEM6, IP5 and the composite log (Short and Long resistivity, Single resistivity, SP and Gamma-ray logs) of well 3 (Figure 17), there is a good match between surface and subsurface geophysical techniques. Therefore, this matching may help to trust these studies, especially in coastal aquifer regions. Also, it is used in calibration between TEM and TDIP methods instead of the other methods.

The registered units from TEMs are five units and their electrical and geological properties are:

➢ **Unit 1**, sand to clayey sand to sandy clay surface layer with low resistivity and high salinity. Its thickness ranges from ~20 m (SE) to ~40 m (NW).
➢ **Unit 2**, clay to sandy clay layer with extremely low resistivity. Its thickness ranges from ~10 m (SE) to ~50 m (NW).
➢ **Unit 3**, sand to clayey sand to sandy clay with low resistivity and high salinity. Its thickness ranges from ~50 m to ~90 (NW), and ~65 m (SE).
➢ **Unit 4**, clay to sandy clay with extremely low resistivity. It starts at depths of ~140 m or ~145 m (NW) and ~95 (SE) and is ~5 m thick. It was recorded only in TEMs 5 and can extend over ~65 m at the NW with sand intercalation.
➢ **Unit 5**, clayey sand low resistivity and high salinity. It was recorded only in (SE) direction at TEMs 5 after depth of ~102 m.
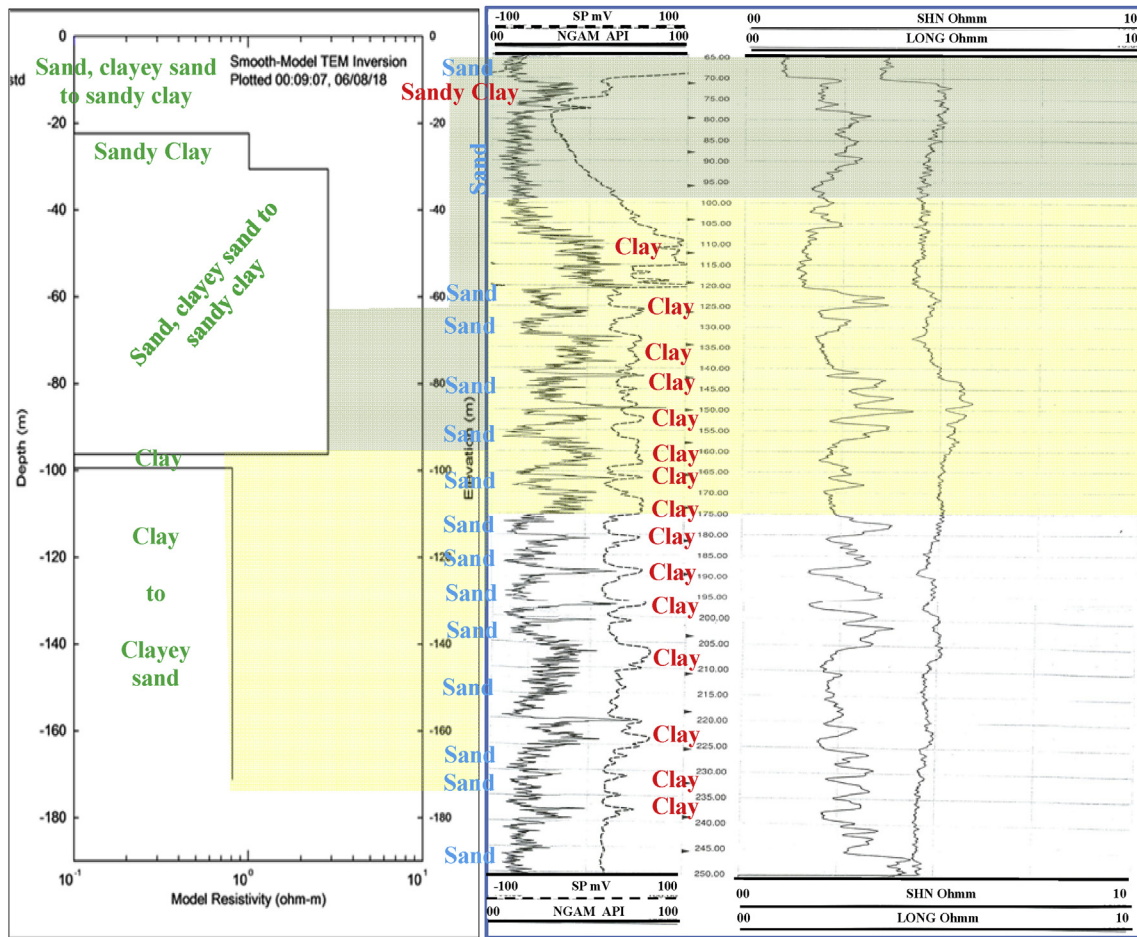
Figure 21. The matching between TEMs5 (left panel) with the composite log (short and long resistivity, SP and gamma ray logs) well (right panel) at same location of TEMs5.

5. Comparing between TDIP and TDEm

From a comparison of the observed chargeability, the calculated depth of the TDIP soundings, and the calculated resistivity with the depth of TEM Soundings, most of TEMs were inverted image or more identical to the IPs, particularly at shallow depths, as shown in Figure 18. This conformity confirms that the two methods are appropriate for use in areas of highly saline water to identify and distinguish between the various subsurface sediments.

6. Comparison of DC resistivity, TDIP and TDEM

A comparison between the observed and calculated chargeability and the calculated resistivity was carried out from VESs (Zohdy and Bisdorf, 1989) and TEMs (using 1D-layered models using *Zonge engineering*) (Figure 19). This comparison is less sufficient between the observed and calculated chargeability and the resistivity of the calculated VESs and TEMs. Therefore, the observed chargeability was competent in separating the different sediments (especially at shallow depths) from the calculated chargeability. The calculated resistivities from VESs and TEMs were less accurate in separating different sediments due to effect of highly conductive layers composed of clay to clayey sediments of highly saline water.

Therefore, the interpretation of TEM and IP soundings helps in identifying and distinguishing between different sedimentary layers. These layers are very complex in their stratigraphy. Generally, it consists of intercalation between sand and clay/silt. So, the above results of TEM and IP are in excellent agreement with the general coastal geological and

hydrogeological model in this area, and previous results of hydrogeological, geological and geophysical studies. However, these sections (individually) would not provide a specific view of salinity, either laterally or with depth, but they were very useful in separating clayey zones from the clean sand zones. The TDIP method was more accurate at separating thin clay layers at shallow depths than the TDEM method. Also, the SP and DC-Resistivity outputs were less accurate in separating the different sediments. Therefore, the resulting inverse model (true resistivity to TEMs) should be used with the observed chargeability to study coastal aquifers with high saline water, clay strata with high concentration of clay intercalated with other sediments.

7. Matching between TEM and composite well logging results

Data support from the geophysical survey was achieved through calibration and qualitative correlation of the resistivity data with information obtained from nearby logged boreholes and geological maps to provide information on the geology of the site especially the complex site of geology (Rucker et al., 2011). Therefore, in this study, calibration and qualitative resistivity correlation, from analyses of TEM data, and chargeability, from analyses of IP data, with well log data including gamma ray and resistivity logs to verify the subsurface geological setting of this area. Martínez et al. (2009) used resistivity data with calibration using geological observations and borehole studies in the coastal aquifer of the Plio-Quaternary Delta sediment deposits to improve the hydrogeological conditions of this aquifer. Also, they used profiles designed to detect the lithological changes, as well as potential horizontal or vertical penetration of seawater intrusion.

Therefore, in this study, the outputs of the inversion model of deep TEMs 1 (resistivities and depths) were calibrated with the composite log (Short and Long resistivity, SP and Gamma ray logs), at same location of TEMS5 as shown in Figure 20. The expected lithology from TEMs 1 is sand, clayey sand to sandy clay to a depth of ~36 m, clay to depth of ~58 m, sand, and clayey sand to sandy clay to ~149 m depth and then clay to clayey sand up to ~207.5 m depth. The interpreted lithology from the composite logs was sand, sandy clay, sand, clay, sand, clay, sand, clay to sand for a depth of ~60–150 m. The last lithology means that the main lithology is sand, sandy clay to minor clayey sand. These depths from ~60 to 150 m in composite logs correspond to depths of 58–149 m in the inversion model of TEMs 1. Also, the interpreted lithology from the composite logs was clay, sand, clay, sand, clay, sand, clay, sand, clay, sand, clay, sand, clay, sand, clay, sand, clay, sand, clay, sand, clay to sand for a depth of ~150–210 m (Figure 20). The main lithology is clay to clayey sand with increase of sand with depth. These depths from ~150 to >210 m in composite logs are in good correlation with depths from 149 to 210 m in the inversion model for TEMs 1.

Likewise, the outputs of the inversion model for TEMs 5 were calibrated with the previous composite log (Figure 21). The expected lithology from TEMs 5 was sand and clayey sand to sandy clay up to a depth of ~31 m. The expected lithology was sand and clayey sand to sandy clay up to ~96 m and clay up to ~99 m then clay to clayey sand up to ~171 m. The interpreted lithology from the composite logs was sand, sandy clay to sand of ~65–~96 m depth. The main lithology is sand and sandy clay to sand. These depths from ~65 to ~96 m in composite logs are in good correlation with depths from 65 to ~96 m with clay at the base (3 m thickness) in the inversion model of TEMs 5. Also, the interpreted lithology from the composite logs was sand, clay, sand, clay, sand, clay, sand, clay, sand, clay, sand, clay, sand, clay from depth ~99–~175 m. The main lithology is clay to clayey sand with increased clay concentration. These depths of ~99–~175 m in composite logs correspond well to depths of 99–175 m in the inversion model of TEMs 5.

8. Conclusion and recommendations

Four surface geophysical techniques have been applied in the research area to investigate the geological and hydrogeological settings as interesting engineering implications at the site of investigation of the coastal areas with emphasis on geological units, soil texture and salinity variation horizontally and vertically with depth. These techniques include shallow geo-electric methods and deep electromagnetic method. The geo-electric methods include SP, DC-Resistivity and TDIP methods while the electromagnetic method includes the TDEM method. The main target here is the distinguish between layers of clay or clayey and sand or sandy layers in different saturated sediments with high salt water and occur between the two major sources of salt water, Mediterranean Sea and Lake Manzla. There were complex lateral and vertical differences in the recorded sediments along study area. Most depths from the surface to about 120 m contain different clay contents and this content increases and sometimes decreases with depth. Confirmed that the subsurface sediments are saturated with highly saline water and there are very slight changes, horizontally and vertically, upon salinity with depth from shallow depths to about 250m.

Due to the geological heterogeneity, as determined from TDIP and TDEM methods with other techniques and the effect of seawater intrusion, it is difficult to precisely delineate the mixing zone of salt water. The subsurface layers are gathered from thin and thick clay strata, silts, clayey sand and sandy clay layers. These layers were recorded at different depths within the study area and were complex in geological and environmental deposits. The predominant matrix in most layers is clay up to ~160 m with unspecified amount of silt intercalation with sand of various sizes. All layers are saturated with highly saline water. The depth of realization was limited to ~210 m due to the effect of high salinity and high clay content. TEM results show a zone of less saline water and low clay content starting from ~40 to ~100 m. There is high to medium clay

content after these depths up to ~250 m. The salinity will increase rapidly after this depth. In the end, it can be said that studies of environmental, geological, and hydrogeological conditions of the areas of highly saline water with clay layers are not easy by conventional methods.

According to the previous results, the technique of both TDEM and TDIP methods are very effective and competent in studying the geological and hydrogeological settings of the high salinity coastal subsurface layers in the coastal zone and also in separating the stratigraphic units and layers. Also, the resistivity method is ineffective in these conditions because it is more affected by the clay content and salinity.

Declarations

Author contribution statement

A.I. Ammar: Conceived and designed the experiments; Performed the experiments; Analyzed and interpreted the data; Contributed reagents, materials, analysis tools or data; Wrote the paper.

M. Gomaa: Contributed reagents, materials, analysis tools or data; Wrote the paper.

K.A. Kamal: Conceived and designed the experiments; Performed the experiments; Wrote the paper.

Data availability statement

Data included in article/supplementary material/referenced in article.

Declaration of interests statement

The authors declare no conflict of interest.

Additional information

No additional information is available for this paper.

References

Alabi, A.A., Ogungbe, A.S., Adebo, B., Lamina, O., 2010. Induced polarization interpretation for subsurface characterization: a case study of obadore, lagos state. Arch. Phys. Res. 1, 34–43.

Balia, R., Ardau, F., Barrocu, G., Gavaudò, E., Ranieri, G., 2009. Assessment of the Capoterra coastal plain (southern Sardinia, Italy) by means of hydrogeological and geophysical studies. Hydrogeol. J. 17, 981–997.

Balia, R., Viezzoli, A., 2015. Integrated interpretation of IP and TEM data for salinity monitoring of aquifers and soil in the coastal area of Muravera (Sardinia, Italy). Boll. Geofis. Teor. Appl. 56 (1), 31–42.

Choudhury, K., Saha, D.K., Chakraborty, P., 2001. Geophysical study for saline water intrusion in coastal alluvial terrain. J. Appl. Geophys. 46, 189–200.

Erol, A.O., 1989. Engineering geological considerations in a salt dome region surrounded by sabkha sediments, Saudi Arabia. Eng. Geol. 26 (3), 215–232.

Everett, M.E., Meju, M.A., 2005. Near-surface controlled-source electromagnetic induction. In: Rubin, Y., Hubbard, S.S. (Eds.), Hydrogeophysics. Water Science and Technology Library, 50. Springer, Dordrecht.

Fitterman, D.V., Deszz-Pan, M., 1998. Helicopter EM mapping of saltwater intrusion in everglades national park, Florida. Explor. Geophys. 29 (1-2), 240–243.

Gemail, K.S., Alfy, M.E., Ghoneim, M.F., Shishtawy, A.M., Abd El Bary, M., 2017. Comparison of DRASTIC and DC resistivity modeling for assessing aquifer vulnerability in the central Nile Delta, Egypt. Environ Earth Sci 76, 350.

Goldman, M., Arad, A., Kafri, U., Gilad, D., Melloul, A., 1989. Detection of freshwater/sea- water interface by the time domain electromagnetic (TDEM) method in Israel. In: Proc. l0th SWIM, Ghent, 1988, pp. 329–344.

Goldman, M., Kafri, U., 2006. Hydrogeophysical applications in coastal aquifers. In: Vereecken, H., Binley, A., Cassiani, G., Revil, A., Titov, K. (Eds.), Applied Hydrogeophysics. NATO Science Series, 71. Springer, Dordrecht.

Goldman, M., Neubauer, F.M., 1994. Groundwater exploration using integrated geophysical techniques. Surv. Geophys. 15, 331–361.

Gross, G.W., Moore, E.J., 1959. Spontaneous polarization potentials and clay and limonite deposits in the Gatesburg Formation of central Pennsylvania. Econ. Geol. 54, 1056–1067.

Kafri, U., Goldman, M., 2005. The use of the time domain electromagnetic method to delineate saline groundwater in granular carbonate aquifers and to evaluate their porosity. J. Appl. Geophys. 57 (3), 167–178.

Kamenetsky, F.M., 1997. Transient geo-electromagnetics. GEOS, moscow. In: Burnett, W.C., Chanton, J.P., Kontar, E.A. (Eds.), Submarine Groundwater Discharge, Biogeochemistry 66, 2003. Kluwer Academic Publishers, The Netherlands, p. 202.

Klitzsch, E., List, F.K., Pohlmann, G., 1987. Geological Map of Egypt. Conoco Coral and Egyptian General Petroleum Company, Cairo, Egypt scale 1:500 000.

Kontar, E.A., Ozorovich, Y.R., 2006. Geo-electromagnetic survey of the fresh/salt water interface in the coastal southeastern Sicily. Continent. Shelf Res. 26 (27), 843–851.

Kruse, S.E., Brudzinski, M.R., Geib, T.L., 1998. Use of electrical and electromagnetic techniques to map seawater intrusion near the Cross-Florida Barge Canal. Environ. Eng. Geosci. IV (3), 331–340.

Magnusson, M.K., Fernlund, J.M.R., Dahlin, T., 2010. Geoelectrical imaging in the interpretation of geological conditions affecting quarry operations. Bull. Eng. Geol. Environ. 69, 465–486.

Manheim, F.T., Krantz, D.E., Bratton, J.F., 2004. Studying groundwater under Delmarva Coastal Bays using electrical resistivity. Ground Water (Oceans issue) 42, 1052–1068.

Marshall, D.J., Madden, T.R., 1959. Induced polarization, a study of its causes. Geophysics 24 (4), 790–816.

Martínez, J., Benavente, J., García-Aróstegui, J.L., Hidalgo, M.C., Rey, J., 2009. Contribution of electrical resistivity tomography to the study of detrital aquifers affected by seawater intrusion–extrusion effects: the river Vélez delta (Vélez-Málaga, southern Spain). Eng. Geol. 108 (3–4), 161–168.

McNeill, J., 1994. Principles and Application of Time Domain Electromagnetic Techniques for Resistivity Sounding. Geonics Ltd. Technical Note TN-27.

McNeill, J.D., 1990. Use of electromagnetic methods for groundwater studies. In: Ward, S.H. (Ed.), Geotechnical and Environmental Geophysics1, Review and Tutorial. Society of Exploration Geophysicists, Tulsa, pp. 191–218.

Nowroozi, A.A., Horrocks, S.B., Henderson, P., 1999. Saltwater intrusion into the freshwater aquifer in the eastern shore of Virginia: a reconnaissance electrical resistivity survey. J. Appl. Geophys. 42 (1), 1–22.

Parks, E.M., McBride, J.H., Nelson, S.T., Tingey, D.G., Mayo, A.L., Guthrie, W.S., Hoopes, J.C., 2011. Comparing electromagnetic and seismic geophysical methods: estimating the depth to water in geologically simple and complex arid environments. Eng. Geol. 117 (1–2), 62–77.

Revil, A., Binley, A., Mejus, L., Kessouri, P., 2015. Predicting permeability from the characteristic relaxation time and intrinsic formation factor of complex conductivity spectra. Water Resour. Res. 51 (8), 6672–6700.

Revil, A., Florsch, N., 2010. Determination of permeability from spectral induced polarization in granular media. Geophys. J. Int. 181 (3), 1480–1498.

Revil, A., Karaoulis, M., Johnson, T., Kemna, A., 2012. Review: some low-frequency electrical methods for subsurface characterization and monitoring in hydrogeology. Hydrogeol. J. 20, 617–658. Springer.

RIGW, 2002. Nile Delta Groundwater Modeling Report. Research Institute for Groundwater, Kanater El-Khairia.

RIGW, 2018. Hydrogeological Investigation for the New Desalination Unit in Port Said Area, North Delta, Egypt. Technical Report. Research Institute for Groundwater.

Rucker, D.F., Noonan, G.E., Greenwood, W.J., 2011. Electrical resistivity in support of geological mapping along the Panama Canal. Eng. Geol. 117 (1–2), 121–133.

Said, R., 1981. The nile in Egypt. In: The Geological Evolution of the River Nile. Springer, New York, NY.

Schön, J.H., 2015. Physical properties of rocks: fundamentals and principles of petrophysics. Dev. Petrol. Sci. 65, 2–497. Elsevier.

Seigel, H.O., 1959. Mathematical formulation and type curves for induced polarization. Geophysics 24 (3), 547–565.

Shah, S., Kress, W., Land, L., 2007. Time-domain Electromagnetic Soundings to Characterize Water Quality within a freshwater/saline-water Transition Zone, Estancia Valley, New Mexico, July 2005—a Reconnaissance Study. USGS Fact Sheet 2007–3011.

Shtivelman, V., Goldman, M., 2000. Integration of shallow reflection seismics and time domain electromagnetics for detailed study of the coastal aquifer in the Nitzanim area of Israel. J. Appl. Geophys. 44 (2-3), 197–215.

Slater, L., Sandberg, S., 2000. Resistivity and induced polarization monitoring of salt transport under natural hydraulic gradients. Geophysics 65 (2), 408–420.

Slater, L.D., Lesmes, D., 2002. IP interpretation in environmental investigations. Geophysics 67 (1), 77–88.

Stewart, M., Gay, M.C., 1986. Evaluation of transient electromagnetic soundings for deep detection of conductive fluids. Ground Water 24 (3), 351–356.

Sumner, J.S., 2012. Principles of Induced Polarization for Geophysical Exploration, 5. Elsevier, Amsterdam, The Netherlands.

Weller, A., Slater, L., Nordsiek, S., 2013. On the relationship between induced polarization and surface conductivity: implications for petrophysical interpretation of electrical measurements. Geophysics 78 (5), D315–D325.

Yang, C., Tong, L., Huang, C., 1999. Combined application of dc and TEM to sea water intrusion mapping. Geophysics 64 (2), 417–425.

Zohdy, A.R., Bisdorf, R.J., 1989. Programs for the Automatic Processing and Interpretation of Schlumberger Sounding Curves in QuickBASIC 4.0.